GEOLOGICAL SURVEY OF CANADA
OPEN FILE 7607

Portable XRF spectrometry of surficial sediment samples in the region of East Arm, Great Slave Lake, Northwest Territories, Canada

B.A. Kjarsgaard, R.D. Knight, A.P. Plourde, and A.M.G. Reynen

2014

Natural Resources Canada | Ressources naturelles Canada

Canada

GEOLOGICAL SURVEY OF CANADA
OPEN FILE 7607

Portable XRF spectrometry of surficial sediment samples in the region of East Arm, Great Slave Lake, Northwest Territories, Canada

B.A. Kjarsgaard[1], R.D. Knight[1], A.P. Plourde[2], and A.M.G. Reynen[2]
[1] Geological Survey of Canada, Ottawa, Ontario
[2] University of Ottawa, Ottawa, Ontario

2014

doi:10.4095/293951

This publication is available for free download through GEOSCAN (http://geoscan.nrcan.gc.ca/).

Recommended citation
Kjarsgaard, B.A., Knight, R.D., Plourde, A.P., and Reynen, A.M.G., 2014. Portable XRF spectrometry of surficial sediment samples in the region of East Arm, Great Slave Lake, Northwest Territories, Canada; Geological Survey of Canada, Open File 7607. doi:10.4095/293951

Publications in this series have not been edited; they are released as submitted by the author.

Table of Contents

Appendices

1.0 Introduction

Over the last decade, the use of portable X-ray fluorescence (pXRF) spectrometry for environmental and exploration geochemistry has grown significantly. Several studies have examined precision, accuracy and calibration of pXRF spectrometers for the examination of soils (e.g., Kenna et al., 2011; McLaren et al., 2011; Weindorf et al., 2012). Morris (2009) provided a data set of pXRF analyses on rock and ore standard reference materials (SRMs), while Knight et al. (2013) provided an extensive data set of pXRF analyses on sediment (till) and silicate-glass reference materials.

This report presents elemental concentrations of till (diamicton) samples collected in 2008 as part of a Mineral and Energy Resource Assessment (MERA) for the proposed Thaidene Nene National Park, located in the area surrounding and to the east of the East Arm of Great Slave Lake, NWT (Fig. 1). The samples utilized for the pXRF analysis were dried and had the pebble and very coarse sand fraction removed prior to analysis (see details in methods section). The pXRF data is compared with 'conventional' geochemistry data for the clay-silt size fraction (< 0.063 mm), determined by ICP-ES/MS analyses following each of lithium borate fusion, 4-acid, and aqua-regia digestion methods (Kjarsgaard et al., 2013a), plus new data obtained in this study for the < 2 mm size fraction (via lithium borate fusion and 4-acid digestion with ICP-ES/MS analysis).

2.0 Sample collection, processing and analytical methods

For this study 241 till samples were analyzed. Till sample sites were determined based on a 10 km x 10 km grid (Kjarsgaard et al., 2013a), resulting in approximately one sample per 100 km^2 (Fig. 2). At each site two samples were collected, a 1 kg sample and an additional 10 to 15 kg sample for heavy mineral analysis, from which a 500 g character split was taken. The 1 kg sample was sent directly to Acme Analytical Laboratories Ltd. (Acme), Vancouver, B.C. for processing (drying, sieving to <0.063 mm), and laboratory geochemical analyses.

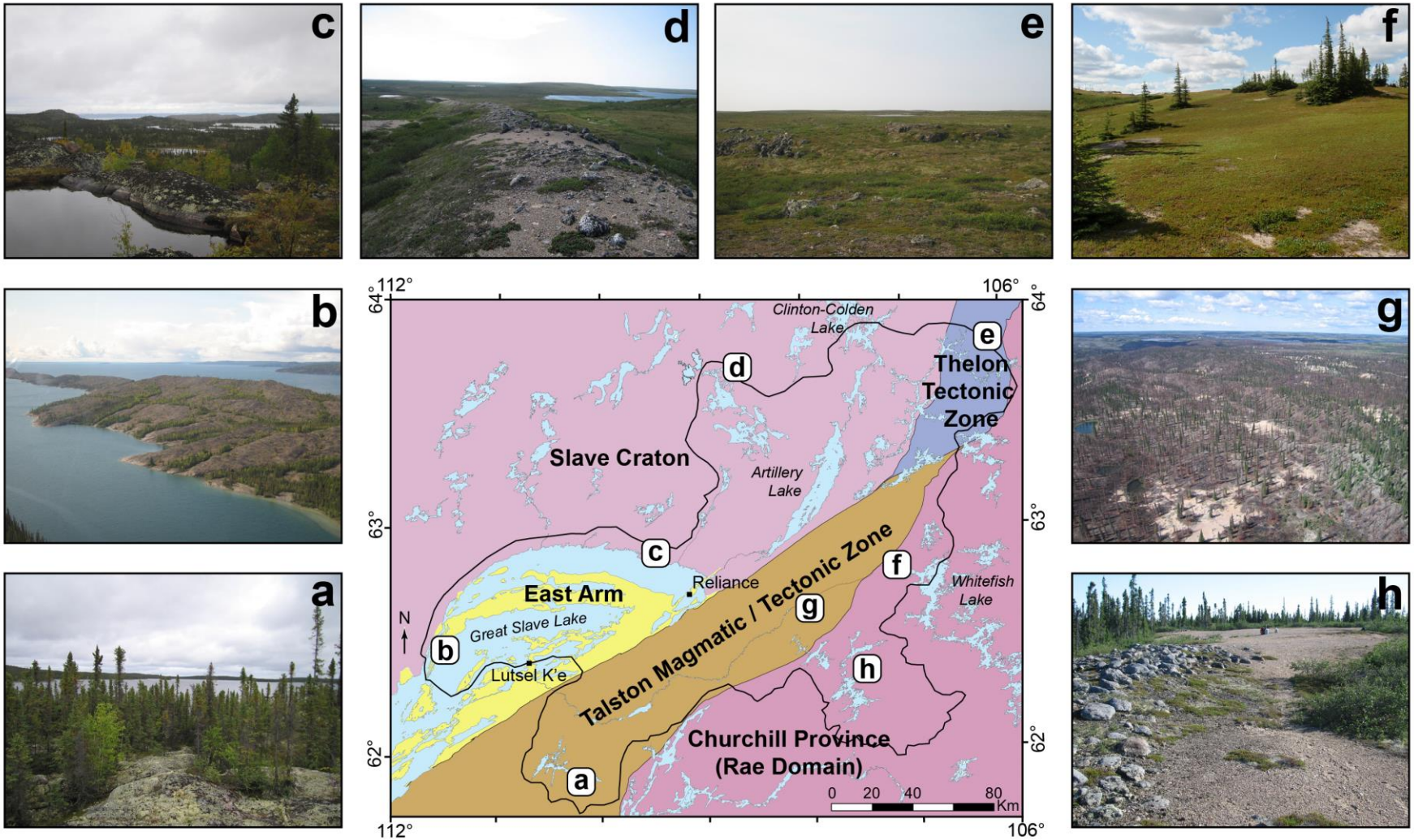

Figure 1. Outline of the study area, and the associated tectonic domains. Letters on the map indicate the location of the photographs that depict the transition from northern boreal forest in the southwest to barrenlands in the northeast. Adapted from Kjarsgaard et al. (2013b).

In preparation for pXRF analysis, a split of the dried but un-sieved till sample used for the geochemical analyses was transferred to a 15 ml plastic vial. The vials were then shaken in order to bring the coarser grained material to the top of the vial through granular convection. This technique is widely used in sedimentology studies (e.g., Wills, 1979), and in industrial processing applications (e.g., Kudrolli, 2004), but this study presents the first documented application of this sample preparation technique to analysis of unconsolidated sediment by pXRF. The coarser material, consisting of pebbles and coarse sand was removed from the top using a small laboratory spatula, with the resultant sample consisting of clay-silt and fine-sand. A 6 μm thick Mylar® polyester film was placed over the plastic vial to separate the sample from the detector.

For the pXRF analyses, a handheld Thermo Scientific Niton XL3t GOLDD XRF spectrometer was utilized, with the instrument mounted in a test stand. The Niton pXRF is equipped with a Cygnet 50 keV, 2 W silver anode X-ray tube, and a XL3 silicon drift detector (SDD) detector with 180,000 counts per second throughput. All analyses were carried out in Soil Mode, which is intended for elemental concentrations < 1%. A dwell time of 60 seconds was used for each of the Main (50 keV, 40 μA max), Low (20 keV, 100 μA max), and High (50 keV, 40 μA max) filters. Six SRMs were analysed at the beginning of each pXRF analytical session, and after approximately every ten samples. Standards included: a SiO_2 blank, CanMet Till-4 (Lynch, 1996), Resource Conservation and Recovery Act (RCRA) 180-436 and NCS 73308, GSC internal till standard TCA 8010 (Girard et al., 2004), and National Institute for Standards and Technology (NIST) 2780 glass (Wilson et al., 1999). A summary of the mean value (based on multiple pXRF analyses of standards) for each element, and their recommended value is presented in Table 1.

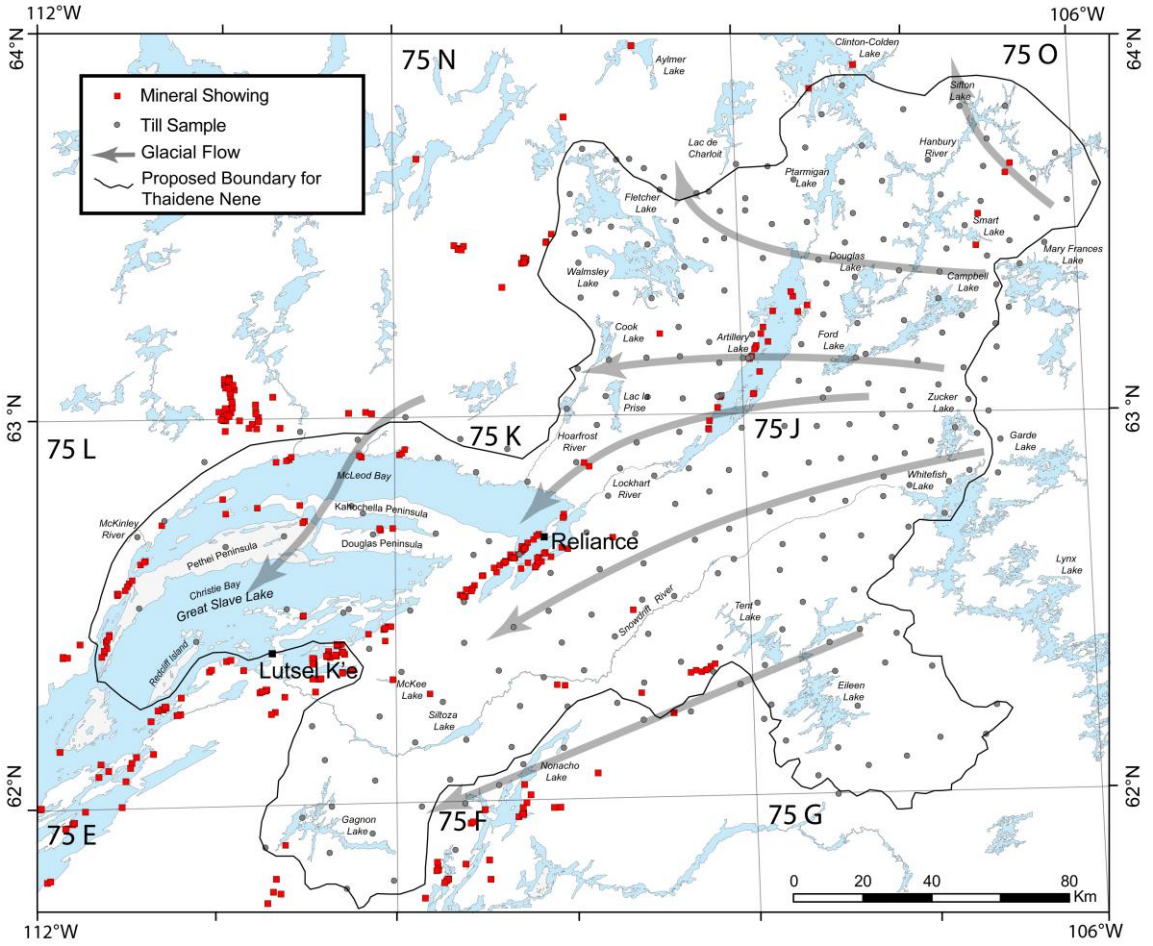

Figure 2. Map of the study area, showing the 2008 field season sample sites, the major lakes and rivers, mineral showings, and main glacial transport direction.

For the laboratory analyses, Acme dried a 500 g split of each 1 kg till sample at 60°C and sieved to < 0.063 mm. Subsequently the < 0.063 mm size fraction was analysed by: (1) aqua regia, a hot (95°C) HNO3-HCl digestion, followed by Inductively Coupled Plasma Mass Spectroscopy (ICP-MS) analysis; (2) 4-acid, a hot dissolution in HNO3-HClO4-HF, taken to dryness and then the residue dissolved in HCl, followed by ICP-ES/MS analysis; (3) fusion, a lithium metaborate/tetraborate fusion (hereby referred to simply as fusion) followed by dilute nitric acid digestion of the fused disc, and analysis by Inductively Coupled Plasma Emission Spectroscopy ICP-ES (major elements) and ICP-MS (trace elements). Additional details are described in Kjarsgaard et al. (2013a). New analytical data was obtained by submitting the samples from the analysed pXRF vials for sieving to < 2 mm and then subsequent powdering in a ceramic shatter box. These

powders where then analysed by ICP-ES/MS after 4-acid digestion, and lithium borate fusion, as detailed above. A complete listing of elements analysed, and their detection limits, for all three methods is presented in Table 2. For all methods, after every twenty-five analyses TCA 8010 was inserted to monitor instrument drift, while after every 50 analyses TCA8010 plus Till-1, -2, -3, and -4 were inserted to monitor precision and accuracy, in addition to instrument drift. These five standards were also analysed at the start and end of each analytical session.

3.0 Bedrock Geology of the Study Area

The bedrock geology of this region of the Canadian Shield is complex. Five major geological domains are known (Fig. 1), including the Archean Slave Craton, the Archean and Paleoproterozoic Rae domain of the Churchill Province, the Paleoproterozoic Thelon and Taltson magmatic-tectonic zones (Tella et al., 2013), and the Paleoproterozoic East Arm Basin (Kjarsgaard et al., 2013c). A generalized and simplified bedrock geology map is shown in Figure 3, based on a 1: 250,000 scale compilation (Kjarsgaard et al., 2013d). The major bedrock geology of the southeast part of the Slave Craton consists of granite, metaturbidite and volcanic rocks with minor gneiss, and mafic and alkaline intrusives, plus dolomite. The Rae domain consists of gneiss and granitoid, with mafic plutons and volcanic rocks, and clastic sequences of the Nonacho Group.

The Thelon consists of ortho- and para-gneiss with granite, and the Taltson by granite with granitoid mylonite and gneiss, and mafic intrusives. The East Arm basin contains mainly sediment-dominated successions, with conglomerate, sandstone, siltstone, mudstone and carbonate sedimentary rocks, mafic sills and dykes, and minor mafic to felsic volcanic rocks and associated intrusions. Approximately 500 mineral occurrences (showings) are known in the study area, comprising a wide variety of deposit types (Fig. 2).

	NCS 73308			NIST 2780			RCRA			TCA 8010			TILL-4			SiO2 Blank		
	Count	Mean	Rec.	Count	Mean	Rec.	Count	Mean	Rec.	Count	Mean	Rec.	Count	Mean	Rec.	Count	Mean	Rec.
Ba	26	78	42	23	869	993	25	493	500	27	598	549	27	390	395	24	44	-
Ca	26	5623	2800	25	5203	1950	25	34049	nr	27	14292	15509	27	8610	8934	26	1162	Trace
Cr	26	185	136	25	42	44	25	466	500	24	22	48.4	27	50	53	-	-	-
Cu	26	24	23	25	169	215	25	55	nr	27	39	28	27	229	237	-	-	Trace
Fe	26	21808	27000	25	23861	27840	25	50742	nr	27	15583	20290	27	36364	39700	25	41	Trace
K	26	931	1041	25	31113	33800	25	19280	nr	27	18103	19094	27	27311	26980	26	186	-
Mn	26	800	1010	23	455	462	25	953	nr	27	322	310	27	447	490	-	-	-
Ni	22	28	nr	23	48	nr	25	65	nr	27	55	17.2	27	39	17	-	-	-
Pb	26	26	27	25	4723	5770	25	496	500	27	15	12.2	27	52	50	-	-	-
Rb	26	7.8	9.2	25	155.2	nr	25	81.5	nr	27	48.6	53.6	27	151.2	161	-	-	-
Sr	26	23	25	25	211	nr	25	180	nr	27	287	310	27	115	109	-	-	-
Th	26	6	nr	22	23	nr	25	14	nr	27	7	5.1	27	50	17.4	-	-	-
Ti	26	1467	1270	25	6365	nr	25	4263	nr	27	2585	2578	27	5097	4840	-	-	Trace
U	11	4	nr	4	7	nr	3	6	nr	2	6	1.1	4	9	5	-	-	-
V	26	125	107	23	252	nr	25	132	nr	27	55	49	27	90	67	7	10	-
Zn	26	42	46	25	1978	2570	25	82	nr	27	34	31.9	27	67	70	2	6	Trace
Zr	26	80	70	25	188	nr	25	248	nr	27	300	272	27	416	385	-	-	Trace

Table 1 Standard reference materials analysed by pXRF spectrometry. Mean is the mean value determined from multiple pXRF analyses. The number of times the standard was analysed is indicated by 'count'. Rec. equals the recommended value for the standard for that element. All values in ppm. SiO_2 blank provided by Thermo Scientific with possible trace elements. nr—no recommended value.

FUSION			**4 Acid**			**Aqua regia**		
Element	Unit	MDL	Element	Unit	MDL	Element	Unit	MDL
SiO2	%	0.01	Ti	%	0.001	Ti	%	0.001
TiO2	%	0.01	Al	%	0.02	Al	%	0.01
Al2O3	%	0.01	Fe	%	0.02	Fe	%	0.01
Cr2O3	%	0.002	Ca	%	0.02	Mg	%	0.01
Fe2O3	%	0.04	Mg	%	0.02	Ca	%	0.01
MnO	%	0.01	Na	%	0.002	Na	%	0.001
MgO	%	0.01	K	%	0.02	K	%	0.01
CaO	%	0.01	P	%	0.001	P	%	0.001
Na2O	%	0.01	S	%	0.04	S	%	0.02
K2O	%	0.01	Li	ppm	0.1	Li	ppm	0.1
P2O5	%	0.01	Rb	ppm	0.1	Rb	ppm	0.1
LOI	%	0.10	Cs	ppm	0.1	Cs	ppm	0.02
TOT/C	%	0.02	Be	ppm	1	Be	ppm	0.1
TOT/S	%	0.02	Ba	ppm	1	Sr	ppm	0.5
Rb	ppm	0.1	Sr	ppm	1	Ba	ppm	0.5
Cs	ppm	0.1	Zr	ppm	0.2	Zr	ppm	0.1
Be	ppm	1	Nb	ppm	0.04	Nb	ppm	0.02
Sr	ppm	0.5	Hf	ppm	0.02	Hf	ppm	0.02
Ba	ppm	1	Ta	ppm	0.1	Ta	ppm	0.05
Zr	ppm	0.1	Y	ppm	0.1	Y	ppm	0.01
Nb	ppm	0.1	Sc	ppm	0.1	Sc	ppm	0.1
Hf	ppm	0.1	V	ppm	1	V	ppm	2
Ta	ppm	0.1	Cr	ppm	1	Cr	ppm	0.5
Y	ppm	0.1	Mn	ppm	2	Mn	ppm	1
Sc	ppm	1	Co	ppm	0.2	Co	ppm	0.1
V	ppm	8	Ni	ppm	0.1	Ni	ppm	0.1
Cr	ppm	14	Cu	ppm	0.02	Cu	ppm	0.01
Co	ppm	0.2	Zn	ppm	0.2	Zn	ppm	0.1
Ni	ppm	20	Pb	ppm	0.02	Pb	ppm	0.01
Cu	ppm	5	Mo	ppm	0.05	Tl	ppm	0.02
Zn	ppm	5	W	ppm	0.1	Mo	ppm	0.01
Pb	ppm	1	As	ppm	0.2	W	ppm	0.1
Mo	ppm	1	Sb	ppm	0.02	As	ppm	0.1
W	ppm	0.5	Bi	ppm	0.04	Sb	ppm	0.02
Ga	ppm	0.5	Ga	ppm	0.02	Bi	ppm	0.02
Sn	ppm	1	Cd	ppm	0.02	B	ppm	20
La	ppm	0.1	Sn	ppm	0.1	Se	ppm	0.1
Ce	ppm	0.1	La	ppm	0.1	Te	ppm	0.02
Pr	ppm	0.02	Ce	ppm	0.02	Ga	ppm	0.1
Nd	ppm	0.30	Pr	ppm	0.1	Ge	ppm	0.1
Sm	ppm	0.05	Nd	ppm	0.1	Cd	ppm	0.01
Eu	ppm	0.02	Sm	ppm	0.1	Sn	ppm	0.1
Gd	ppm	0.05	Eu	ppm	0.1	In	ppm	0.02
Tb	ppm	0.01	Gd	ppm	0.1	La	ppm	0.5
Dy	ppm	0.05	Tb	ppm	0.1	Ce	ppm	0.1
Ho	ppm	0.02	Dy	ppm	0.1	Pr	ppm	0.02
Er	ppm	0.03	Ho	ppm	0.1	Nd	ppm	0.02
Tm	ppm	0.01	Er	ppm	0.1	Sm	ppm	0.02
Yb	ppm	0.05	Tm	ppm	0.1	Eu	ppm	0.02
Lu	ppm	0.01	Yb	ppm	0.1	Gd	ppm	0.02
Th	ppm	0.2	Lu	ppm	0.1	Tb	ppm	0.02
U	ppm	0.1	Th	ppm	0.1	Dy	ppm	0.02
			U	ppm	0.1	Ho	ppm	0.02
			Au	ppm	0.1	Er	ppm	0.02
			Ag	ppb	20	Tm	ppm	0.02
						Yb	ppm	0.02
						Lu	ppm	0.02
						Th	ppm	0.1
						U	ppm	0.1
						Pd	ppb	10
						Ag	ppb	2
						Re	ppb	1
						Pt	ppb	2
						Au	ppb	0.2
						Hg	ppb	5

Table 2. Listing of elements analysed, units of measurement, and their detection limits for Fusion, 4-Acid, and Aqua regia methods. MDL (minimum detection limit).

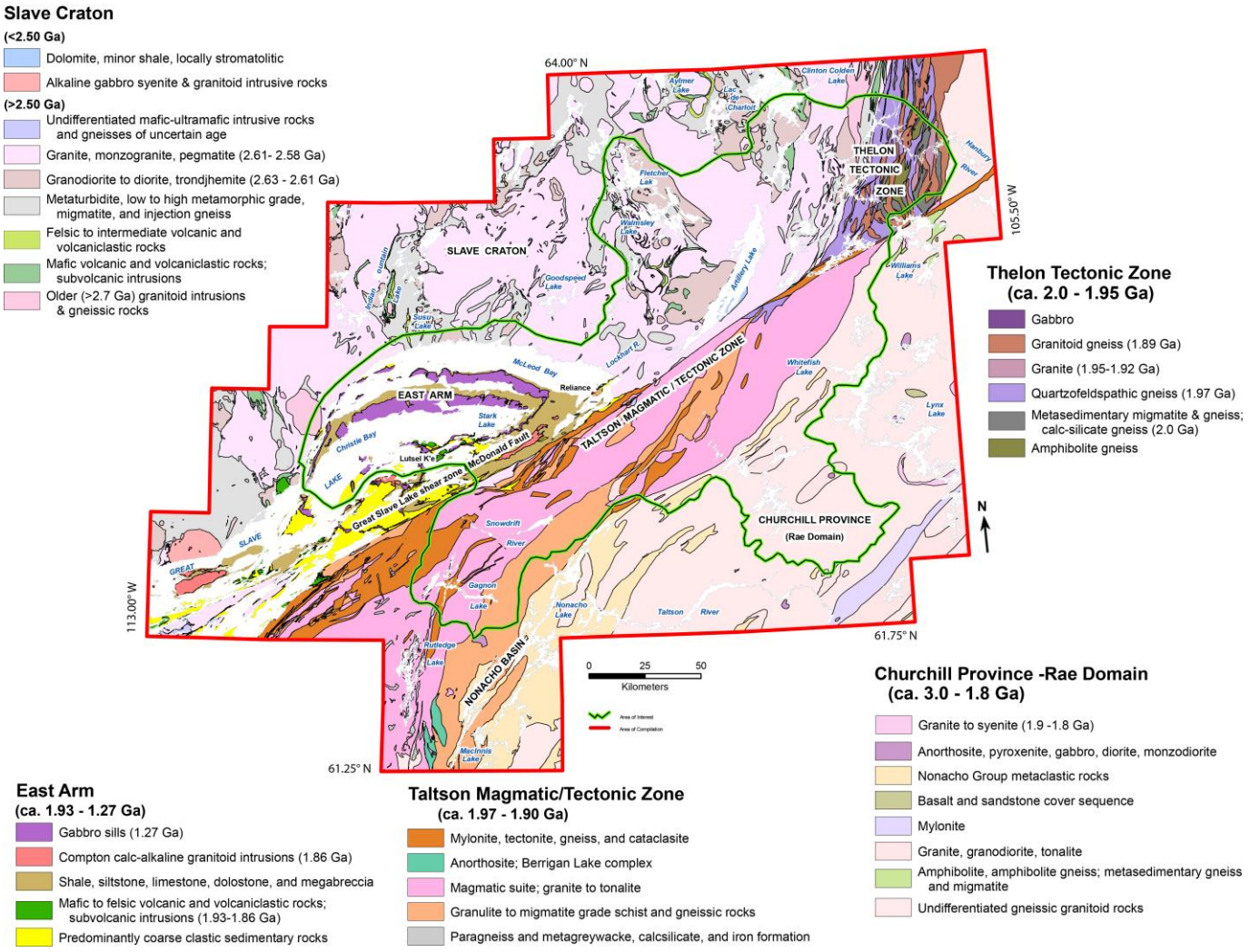

Figure 3. Generalized and simplified bedrock geology map based on a 1: 250,000 scale compilation by Kjarsgaard et al. (2013d).

4.0 Surficial Geology of the Study Area

The proportion and thickness of the surficial cover increases from west-southwest to east - northeast (Fig. 4). The till is a matrix-supported diamicton, which becomes more silica (quartz) rich and sandy in nature from west to east (Kjarsgaard et al., 2013a, e; Kerr et al., 2013a). In the west, bedrock or bedrock with thin till comprises the topographic surface. To the north and east, till veneer (< 2 m), till blanket (2 to 5 m) and hummocky till (> 3) dominate, with much less bedrock or bedrock with till veneer (Kerr et al., 2013a). A regularly spaced (~ 10 km) network of eskers is observed, with glaciofluvial flow direction from east to west. In the study area there are two main recognized glacial ice flow directions, however, there is only one significant transport direction for both glacial and glaciofluvial sediments, which is east to west (Fig. 2; Sharpe et al., 2013). The study area spans the transition from northern boreal forest in the south and southwest to barren lands tundra in the north and northeast (Fig. 1 photographs).

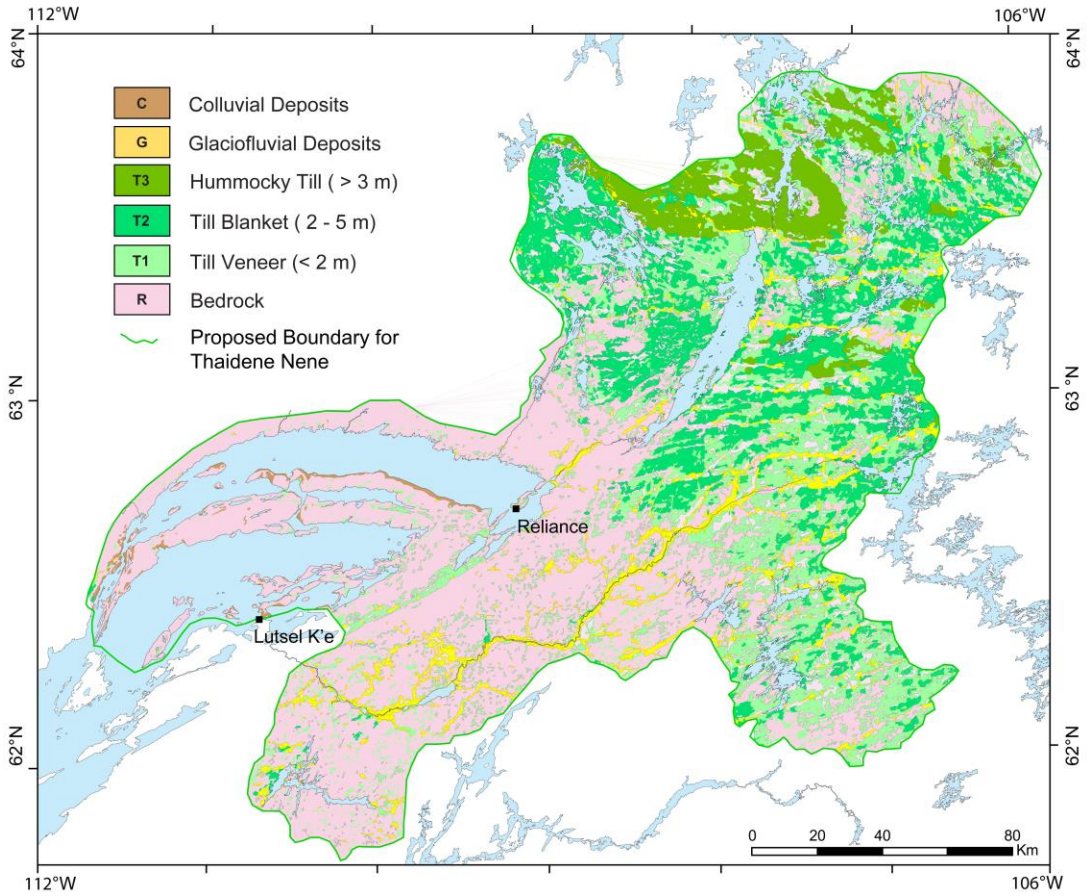

Figure 4. Surficial geology map of the study area (modified from Kerr et al., 2013b).

5.0 Results

Elemental concentrations determined by pXRF analysis, as well as by fusion and 4-acid for the < 2 mm size fraction are listed in Appendix A. Also included in Appendix A are the pXRF data of the five SRM's analysed during the study, and the previously published (Kjarsgaard et al., 2013a) analytical data from fusion, 4-acid, and aqua regia digestions for the < 0.063 mm (clay-silt) size fraction.

For the bivariate plots, a one-to-one relationship is plotted as a dashed red line. Linear regression lines determined by the least squares approach to the data are displayed on the figures in black. Due to 'clusters' of points within the dataset, the regression lines are more dependent on the location of the clusters, rather than the overall shape of the data. For strongly 'clustered' data, the regression lines occasionally deviated from the expected trend. Thus, regression lines were also plotted using a reduced major axis (RMA) method (York, 1966), which Weltje and Tjallingii (2008) used for calibration of data obtained from an XRF core scanner. The RMA regression lines are plotted on the figures in blue. The RMA method is typically used for data sets where both axes values have uncertainty. For this regression method the units of the axes must be the same and the order of magnitude of the uncertainty is required to be similar, which is the case for the datasets presented here. The RMA regression method uses the centroid as the new origin and a covariance matrix is created. The eigenvector corresponding to the larger eigenvalue from this covariance matrix is used to define the direction of the greatest variability. A regression line is plotted using the slope of the eigenvector and the mean coordinates of the dataset.

5.1 Comparison of laboratory data utilizing fusion and 4-acid analytical methods on the < 2 mm, and the < 0.063 mm size fraction of till samples

The main objective of this study is to compare to results from pXRF spectrometry with results from conventional laboratory analytical methods. Since pXRF is a 'total' analysis (for the elements that can be detected or analysed for), we are interested to understand how concentration data obtained from analyses by fusion ('total') and 4-acid ('near total')

digestion methods compare with pXRF spectrometry results. In order to accomplish this we first compare the fusion and 4-acid data sets. Bivariate plots (fusion versus 4-acid) were generated for eighteen elements (Al, Ba, Ca, Cr, Cu, Fe, K, Mn, Ni, Pb, Rb, Sr, Th, Ti, U, V, Zn, and Zr), for the < 2 mm, and the < 0.063 mm size fractions (Appendix B).

Bivariate plots were not generated utilizing the partial dissolution aqua regia digestion data, since it is not a valid comparison to the fusion data (total analysis) or the 4-acid data (near total analysis). In theory, for any element, the fusion ('total analysis') concentration should be equal to or greater than the 4-acid ('near total') concentration. This of course will not be the case for elements that reside in minerals that may not be fully digested by the 4-acid method (e.g., chromite, zircon). The problem with comparing aqua regia data to pXRF data is that 'apparent' higher concentrations levels (i.e., relative concentration levels) can be observed, for elements that dominantly reside in minerals that are easily digested by aqua regia, but only form a small percentage of the overall composition of the material being analysed. Thus elemental concentration levels determined by aqua regia data can be higher, or lower, than that obtained by fusion. As an example, the pXRF versus aqua regia bivariate scatterplots for Cu, Pb and Zn for Pine Point tills presented in Hall and McClenaghan (2013) illustrates the problem using aqua regia data for comparative purposes. Their data illustrates that Cu values by pXRF are ~2X higher than the aqua regia data, Zn data by pXRF and aqua regia are similar, and Pb pXRF data may be either 10's to 100's of ppm higher or lower than the aqua regia data.

From this study, concentration levels for barium are similar for the two digestions, regardless of grain size (Fig. 5). The elements titanium, potassium, rubidium and manganese also exhibit similar characteristics to barium (Appendix B). Concentration levels for iron are similar for the two digestion methods for the < 0.063 mm size fraction, however, for the < 2 mm size fraction concentration levels are slightly higher as determined by the fusion method (Fig. 6). The elements calcium and lead exhibit similar characteristics to iron, however lead data are more scattered, especially for the < 2 mm size fraction (Appendix B). Concentration levels for strontium by either analytical method are similar for the < 2 mm size fraction, however, for the < 0.063 mm size

fraction concentration levels are higher as determined by the fusion method (Fig. 7). The elements thorium and uranium exhibit similar characteristics to strontium (Appendix B). For Sr, Th, U these results suggest these elements reside in minerals that are smaller than < 0.063 mm and are not completely digested using the 4-acid method.

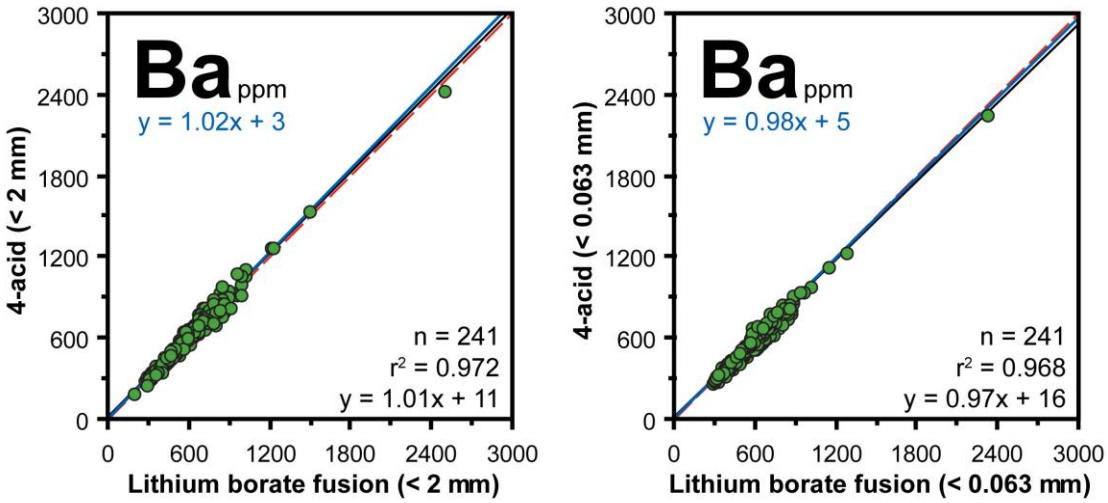

Figure 5. Comparison of elemental concentration as a function of laboratory method (fusion versus 4-acid) for the < 2 mm and < 0.063 mm size fractions for Ba.

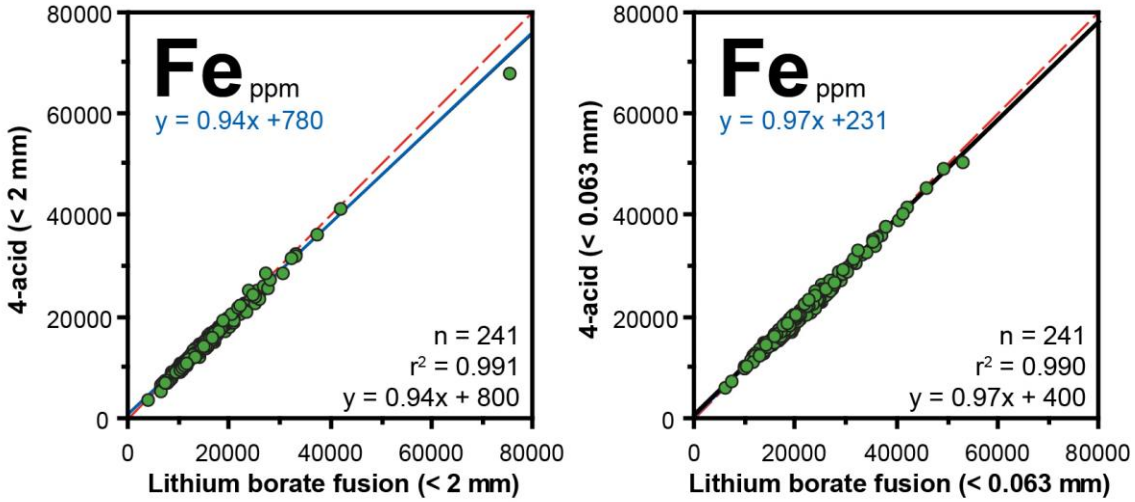

Figure 6. Comparison of elemental concentration as a function of laboratory method (fusion versus 4-acid) for the < 2 mm and < 0.063 mm size fractions for Ba.

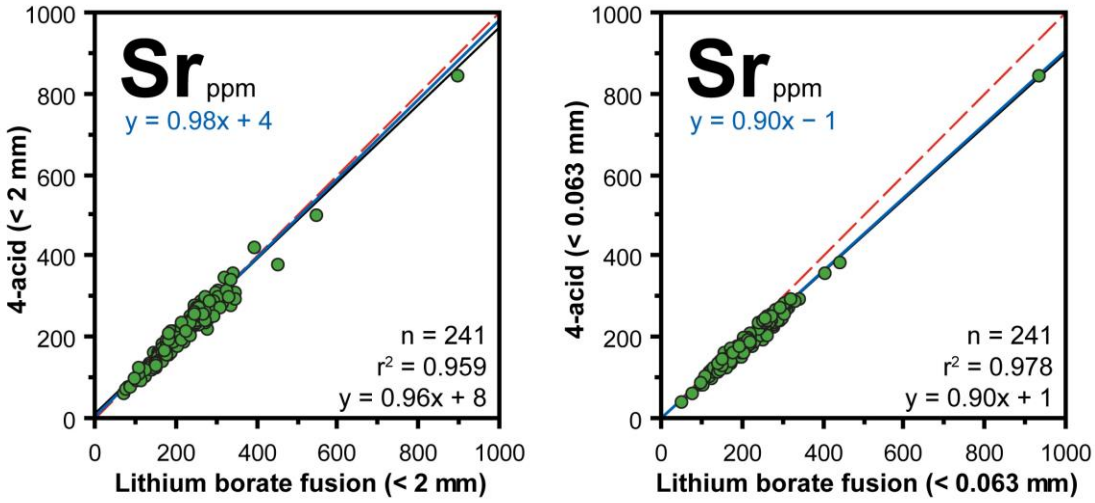

Figure 7. Comparison of elemental concentration as a function of laboratory method (fusion versus 4-acid) for the < 2 mm and < 0.063 mm size fractions for Sr.

Higher concentration levels for zirconium (Fig. 8) and chromium (Appendix B) are observed by the fusion method, regardless of grain size. Higher concentration levels for zinc are observed by the 4-acid method for both grain sizes, but this is more pronounced in the < 0.063 mm size fraction (Fig. 9). The 4-acid and fusion concentration levels of copper are similar for the < 0.063 mm size fraction (Fig. 10). However, for the < 2 mm size fraction, the fusion concentrations are greater, and the data are also highly scattered, with an indication that there may be two populations of Cu data points (Fig. 10). Although there is a paucity of nickel data (> 65% of the samples are below the detection limit by the fusion method), we observe that for the < 2 mm size fraction the concentration levels as determined by fusion are generally higher than those determined by 4-acid, which is suggested to be a result of incomplete dissolution of larger (> 0.063 mm) minerals that are Ni-bearing. For the Ni < 0.063 mm size fraction there is significant scatter, but a higher proportion of the data lies adjacent to the 1:1 reference line as compared to the < 2 mm size fraction (Appendix B).

In summary, we suggest that the fusion method is the preferred laboratory method for comparison with pXRF data for the elements Al, Ba, Ca, Cr, Fe, K, Mn, Rb, Sr, Th, Ti, U, V and Zr, given the concentration levels of the sample suite. For Cu, Pb, Zn and Ni we suggest that the 4-acid method is the preferred laboratory method for comparison with

pXRF data. For these elements, the detection limit by the 4-acid method is lower than by fusion. For example, the Ni concentration levels of the sample suite are low, and there is a highly reduced sample subset (n= 57/241, n = 79/241) for the fusion method, which is a function of the higher detection limit (20 ppm of Ni). The suggested preferred laboratory analytical methods for each element as noted above is similar to those derived by Kjarsgaard et al. (2013a), in which the fusion, 4-acid and aqua regia laboratory methods for the < 0.063 mm size fraction where compared.

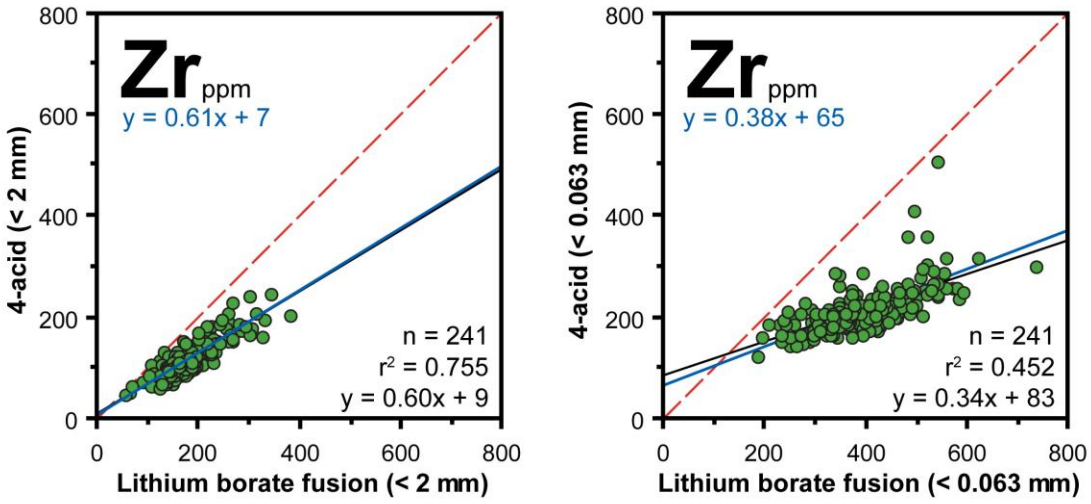

Figure 8. Comparison of elemental concentration as a function of laboratory method (fusion versus 4-acid) for the < 2 mm and < 0.063 mm size fractions for Zr.

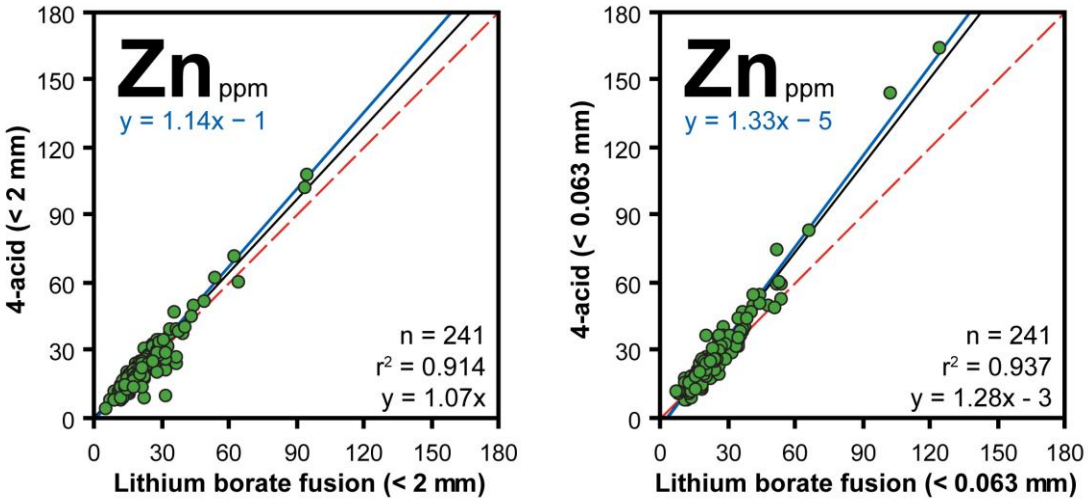

Figure 9. Comparison of elemental concentration as a function of laboratory method (fusion versus 4-acid) for the < 2 mm and < 0.063 mm size fractions for Zn.

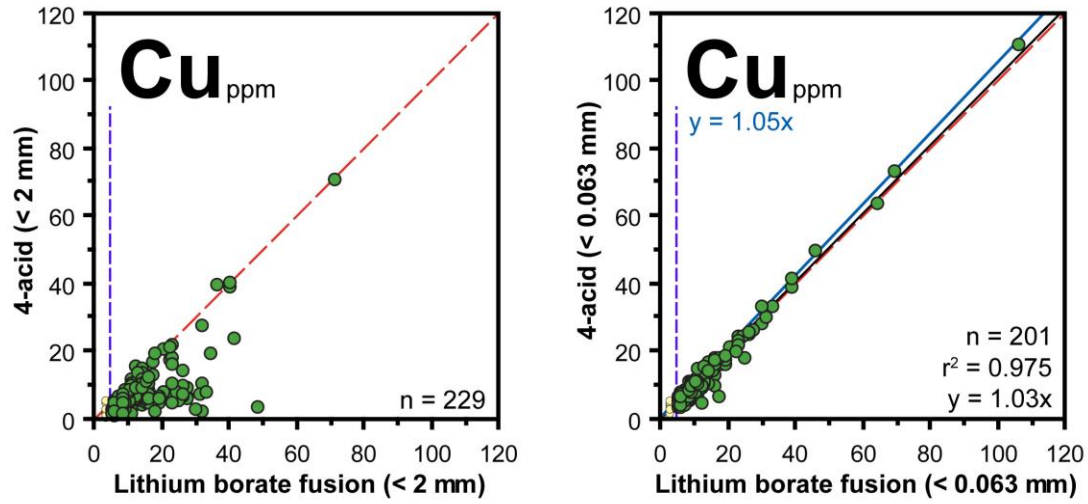

Figure 10. Comparison of elemental concentration as a function of laboratory method (fusion versus 4-acid) for the < 2 mm and < 0.063 mm size fractions for Cu.

5.2 Comparison of the < 2 mm and < 0.063 mm size fractions for fusion and 4-acid method

The grain size of the samples analysed by pXRF spectrometry is silt plus clay, with some fine sand-sized material (i.e., overall grain size is > 0.063 mm and << 2 mm). Thus for comparative purposes we are interested in the variation of chemical composition for the two size fractions, since these size fractions bracket that of the analysed pXRF samples. In order to facilitate the comparison, bivariate plots were generated with the preferred

laboratory digestion method for each of the 18 elements: Al, Ba, Ca, Cr, Fe, K, Mn, Rb, Sr, Th, Ti, U, V and Zr by fusion analyses, and Cu, Ni, Pb and Zn by 4-acid analyses (Appendix B).

The majority of the individual element data at the concentration levels of the sample suite lie adjacent to the 1:1 reference line, suggesting there is little variation between the < 2 mm and < 0.063 mm data sets (Figs. 11, 12). From a statistical perspective, this can be quantified by the equation for the slope of the regression line, and the significance of the fit of the data to the regression line (r^2). For 16 of the elements, r^2 is greater than 0.46,

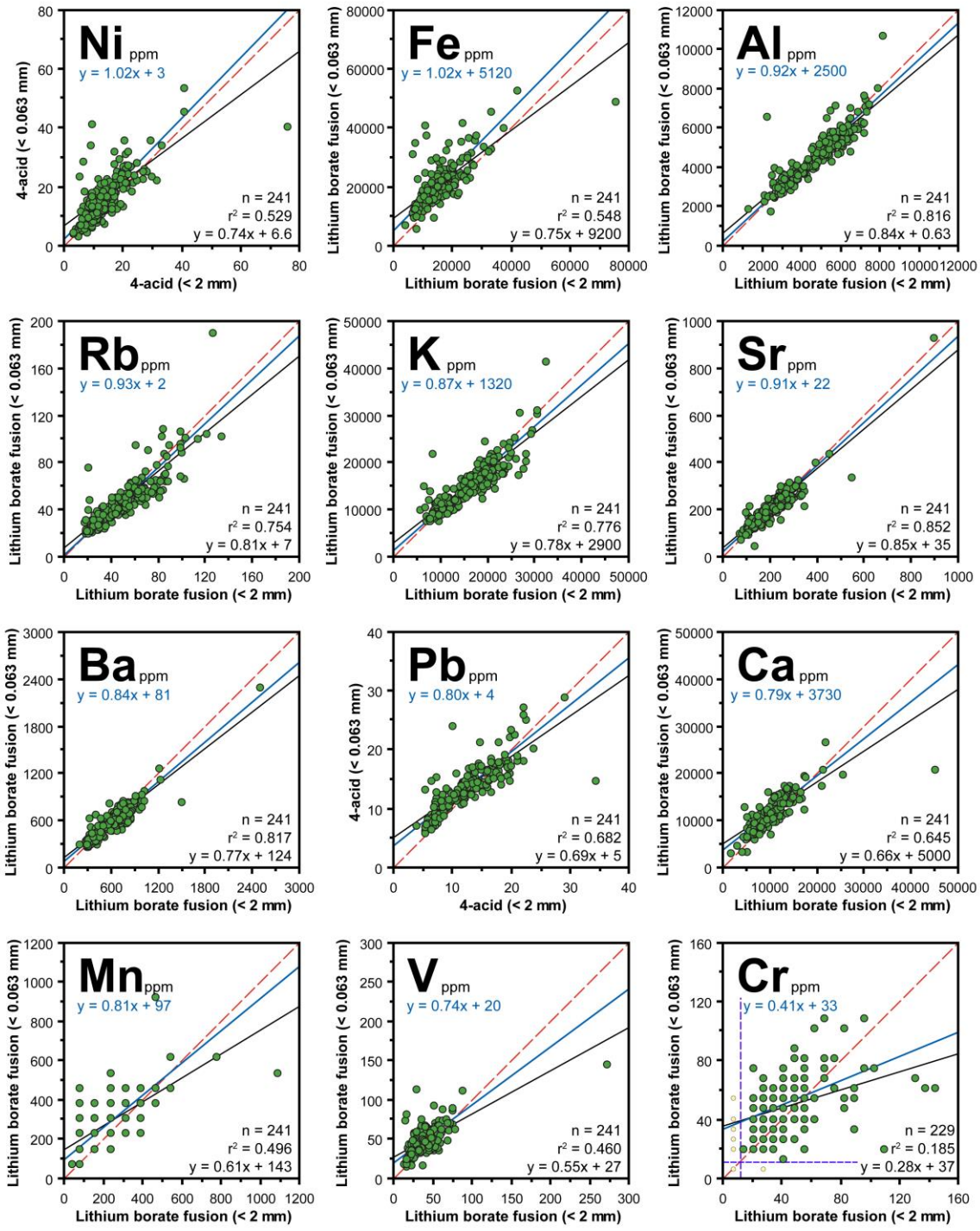

Figure 11. Comparison of elemental concentration as a function of size fraction utilizing either fusion (or 4-acid) digestion for Ni (4A), Fe, Al, Rb, K, Sr, Ba, Pb (4A), Ca, Mn, V and Cr. Purple dashed lines represent the detection limit (DL). Yellow dots represent samples plotted below the DL.

.

which is considered significant given the sample population of 241 (Lemaitre, 1982). However, there is a subset of elements where this is not the case. For zirconium, the data is highly scattered, which precludes fitting a regression line. Chromium data is also scattered, with an r^2 value of 0.185. For titanium, r^2 is 0.477, but the < 0.063 mm concentrations are higher than the < 2 mm. The element suite can be subdivided into two sets, those with higher or tendencies to higher concentrations in the < 2 mm size fraction (Al, K, Rb, Ba, Ca, Sr, Fe, Ni, Pb, Mn, V, Cr; Fig. 11), and those with higher or tendencies to higher concentrations in the < 0.063 mm size fraction (Zr, Cu, Zn, U, Th, Ti; Fig. 12). In the first group, Ni and Fe data cluster along the 1:1 reference line (Fig. 11). For the remaining elements of this group, Al, Rb, Sr, K, Ba, Pb, Ca, Mn, V, Cr (in the order listed), there is an increasing tendency towards higher concentration in the < 2 mm size fraction than the < 0.063 mm, and for this difference to increase at higher concentration levels (Fig. 11). In the second group, titanium and thorium typically exhibit marginally higher concentration levels in the < 0.063 mm size fraction, but all data points lie proximal to the 1:1 reference line.

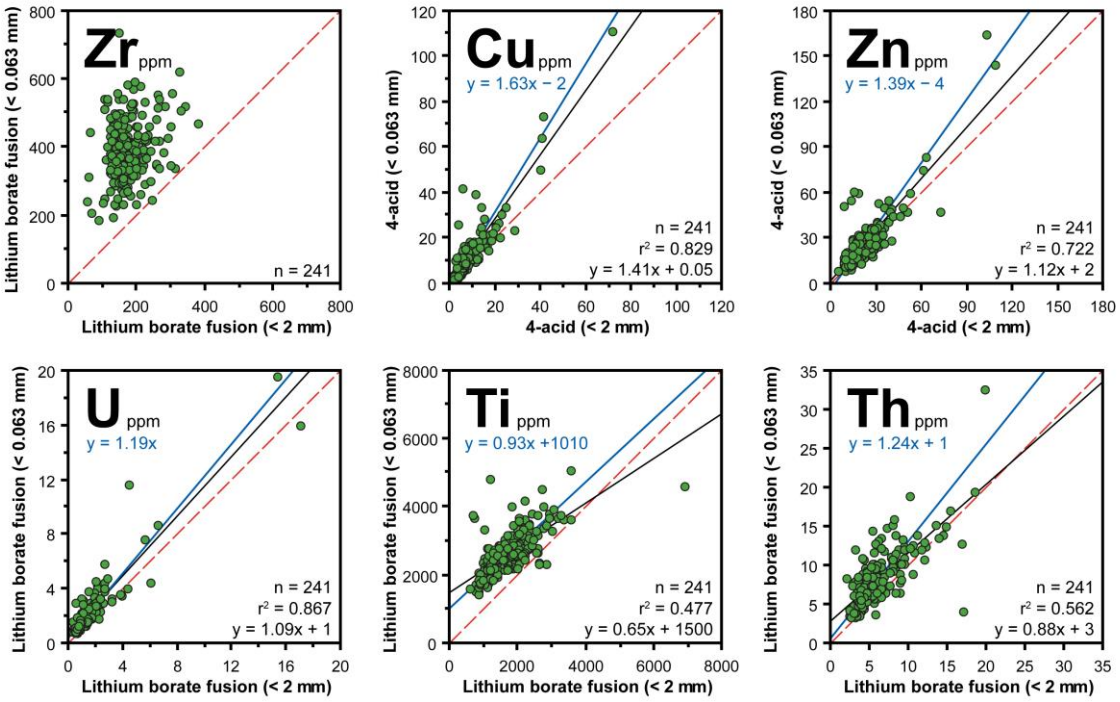

Figure 12. Comparison of elemental concentration as a function of size fraction utilizing either fusion (or 4-acid) digestion for Zr, Cu (4A), Zn (4A), U, Th and Ti.

For the elements U, Zn, Cu and Zr (in the order listed), there is an increasing tendency towards higher concentration in the < 0.063 mm size fraction than the < 2 mm, and for this difference to increase at higher concentration levels (Fig. 12).

5.3 Comparison of pXRF spectrometry data with laboratory analytical data

Portable XRF data for seventeen elements (Ba, Ca, Cr, Cu, Fe, K, Mn, Ni, Pb, Rb, Sr, Th, Ti, U, V, Zn, and Zr) are compared to laboratory analytical data from fusion and 4-acid digestions on the < 2 mm and < 0.063 mm size fractions of the till samples. All pXRF data is listed in Appendix A. A complete set of bivariate scatter plots were generated (Appendix C), including:

(1) Comparison of pXRF data with the < 2 mm fusion data;
(2) Comparison of pXRF data with the < 0.063 mm fusion data;
(3) Comparison of pXRF data with the < 2 mm 4-acid data;
(4) Comparison of pXRF data with the < 0.063 mm 4-acid data.

The following interpretation consists of a comparison of pXRF data with laboratory data utilizing the preferred laboratory digestion method, as outlined above. Thus the pXRF data is compared to the fusion data for 13 elements (Ba, Ca, Cr, Fe, K, Mn, Rb, Sr, Th, Ti, U, V and Zr), and the 4-acid data for 4 elements (Cu, Pb, Zn and Ni), for both size fractions.

The elements K and Rb (alkali metals), Ca, Sr and Ba (alkali earth metals), V and Mn (transition metals) and Pb all have very similar characteristics in terms of pXRF concentration level with respect to the fusion data, and the 4-acid data, for both size fractions (Figs. 13, 14). All r^2 values for the regression lines on these plots are greater than 0.697 and are considered significant, given the size of the sample suite. Bivariate plots of pXRF concentration versus the fusion or 4-acid data, for both the < 2 mm and < 0.063 mm size fractions are dominated by data points that lie along and adjacent to the 1:1 reference line (Figs. 13, 14). However, the pXRF data appears to slightly underestimate concentration levels compared to the < 0.063 mm size fraction laboratory

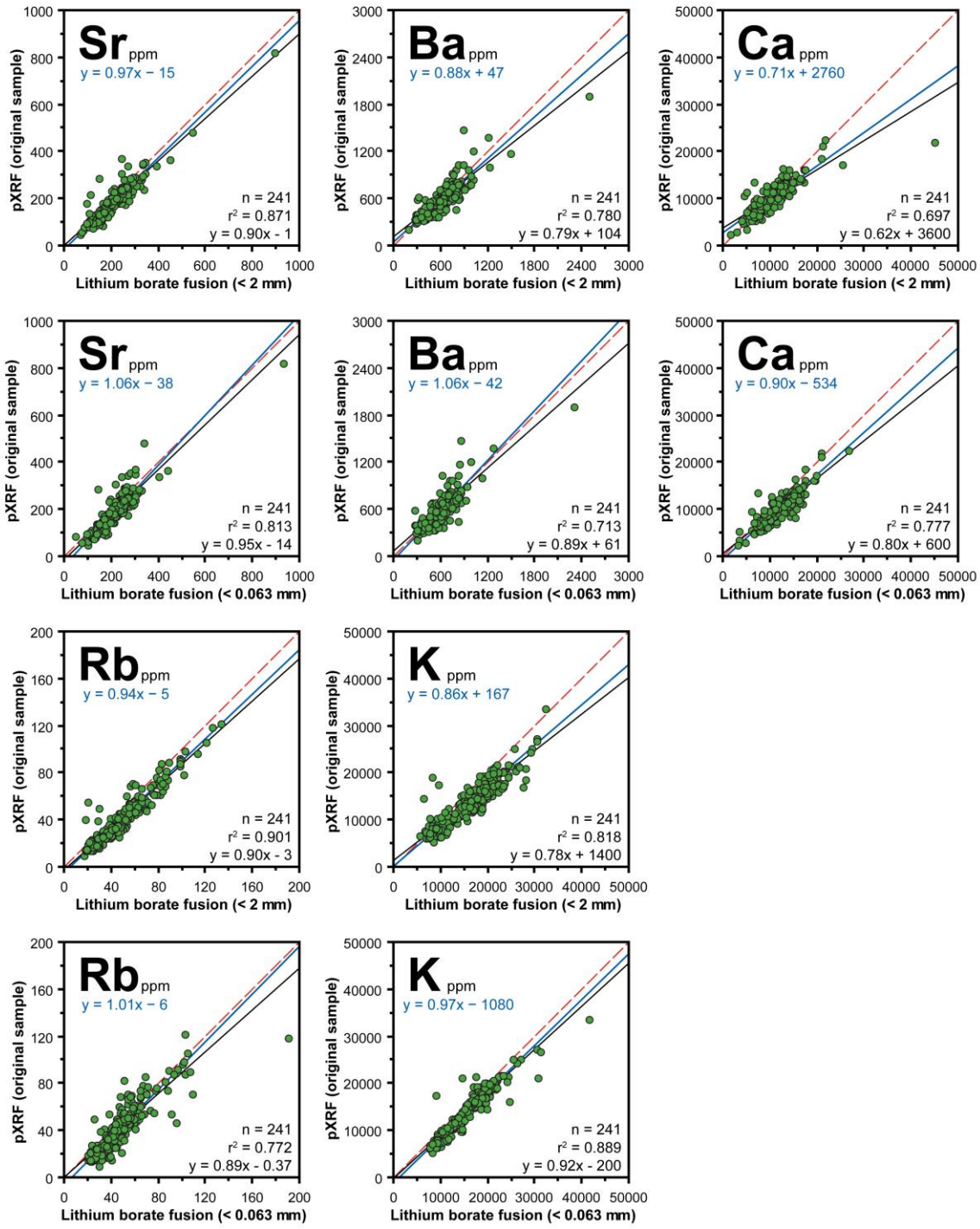

Figure 13. Comparison of pXRF data with fusion data sets for the < 2 mm and < 0.063 mm size fractions for Sr, Ba, Ca, Rb and K.

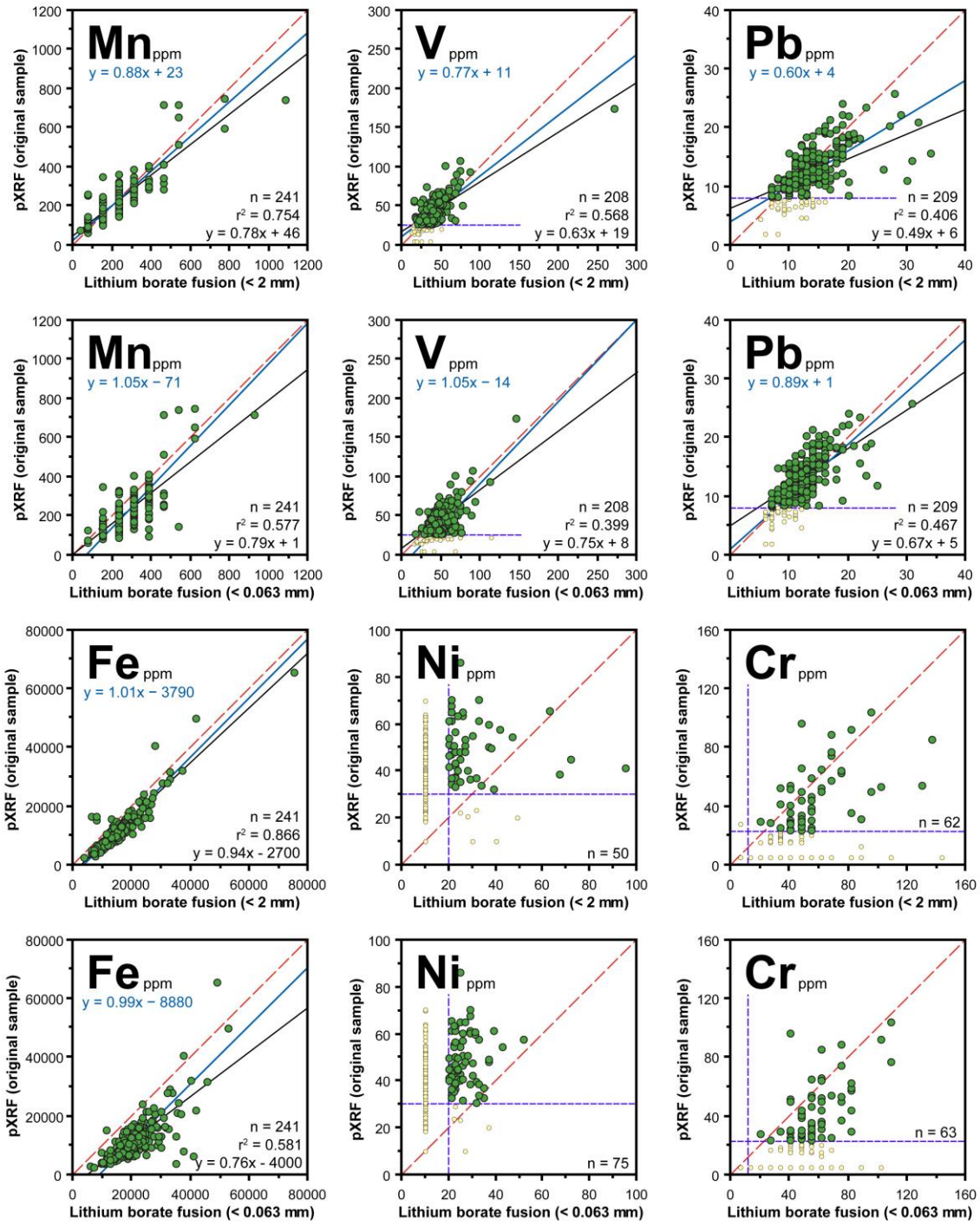

Figure 14. Comparison of pXRF data with fusion data (or 4-acid) sets for the < 2 mm and < 0.063 mm size fractions for Mn, V, Pb (4-acid), Fe, Ni (4-acid) and Cr. Purple dashed lines represent the detection limit (DL). Yellow dots represent samples plotted below the DL.

data, with this effect being slightly more pronounced in comparison with the < 2 mm size fraction data (Figs. 13, 14), as illustrated by the regression line for these elements having rotated clockwise on the < 2 mm scatterplot as compared to the < 0.063 mm scatterplot. The observation that the pXRF is slightly underestimating the concentration level is interpreted to be due to peak interference, or matrix effects. Iron by pXRF exhibits lower concentration levels as compared to the fusion data for either size fraction, with more than ≈95% of the data to the right of the 1:1 reference line (Fig. 14). However, in contrast to the elements listed above, the pXRF Fe data for the two size fractions is quite similar, which is consistent with the fusion < 2 mm versus fusion < 0.063 mm scatterplot (Fig. 11). Cr pXRF data exhibits significant scatter for both grain sizes, but the pXRF appears to underestimate concentration at these low levels (Fig. 14). This is due to ≈75% of the sample set having Cr concentrations levels that are below the pXRF or the fusion detection limit, or, low Cr concentration levels (≤ 3X the detection limit). For Ni concentrations there is little difference between pXRF data for the two size fractions (Fig. 14), consistent with the 4-acid < 2 mm versus 4-acid < 0.063 mm scatterplot (Fig. 11). However, the concentration of Ni determined by pXRF is higher than the 4-acid data for either size fraction (Fig. 14) i.e. the pXRF is overestimating the Ni concentration.

Cu concentrations determined by pXRF are slightly elevated compared to the fusion data, for both size fractions, but much of the data is scattered about the 1:1 reference line at low concentration (Fig. 15). Bivariate plots of Zn, Ti and Th are dominated by data points that cluster adjacent to the 1:1 reference line (Fig. 15), with the Th data exhibiting increased scatter. For all these elements, however, the pXRF appears to slightly underestimate concentration levels in the < 0.063 mm size fraction, with this effect being less pronounced in the < 2 mm size fraction (Fig. 15), as illustrated by the regression line for these elements having rotated counter-clockwise on the < 2mm plot as compared to the < 0.063 mm plot. The elements Zr and U exhibit similar characteristics to Zn, Th and Ti (Fig. 15), but, ≈ 90% of the U pXRF data is below detection limit, and the Zr < 0.063 mm plot exhibits significant scatter, which does not allow for a more robust interpretation.

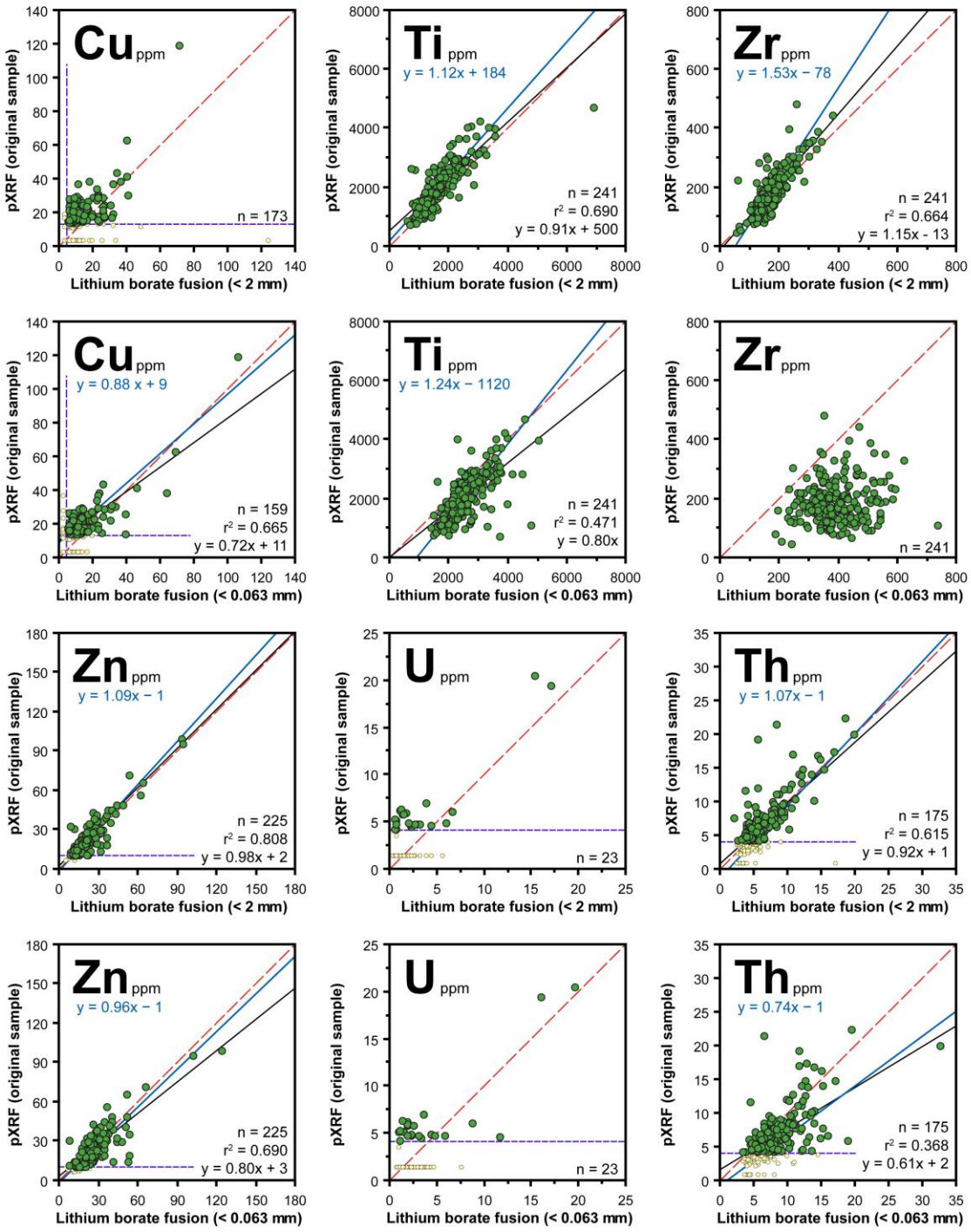

Figure 15. Comparison of pXRF data with fusion and 4-acid data sets for the < 2 mm and < 0.063 mm size fractions Cu (4-acid), Ti, Zr, Zn (4-acid), U and Th. Purple dashed lines represent the detection limit (DL). Yellow dots represent samples plotted below the DL.

In summary, using the methods presented here, pXRF spectrometry for Sr, Ba, Ca, Rb, K, Fe, Mn, V, Ti, Cu, Pb, Zn is considered acceptable, based on the comparison to the preferred laboratory digestion method (either fusion data, or 4-acid data) for each element.

Post-analysis correction of data for these elements does not provide significant additional insights to the data set (e.g., for K; Fig. 16). For, Ni, Cr and U (both size fractions), and Th and Zr (< 0.063 mm) there is a much higher degree of scatter and regression lines where not determined. For these elements it would be useful to post-analysis correct the data, especially if they systematically deviate from the 1:1 reference line (e.g., Ni, Fig. 14). However, the standard reference materials utilized in this study (Table 1) do not provide an appropriate number, nor range of concentration data, to construct a standards-derived Ni regression line for the post-analysis correction. In hindsight, this highlights the importance of careful selection of standard reference materials that span the complete list of elements and concentration levels that can be detected and are of interest.

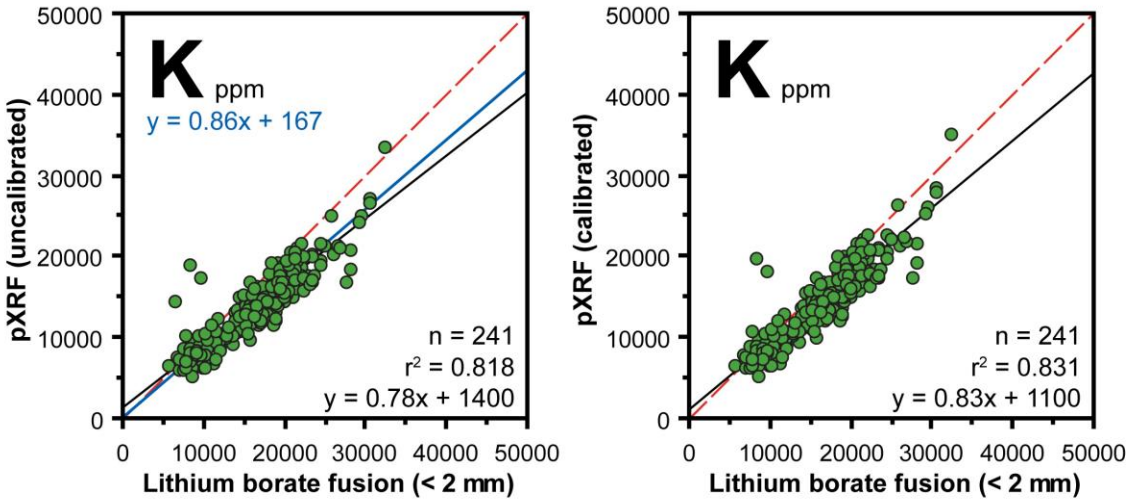

Figure 16. Comparison of raw pXRF and post-analysis corrected concentration data for K with fusion data sets for the < 2 mm and < 0.063 mm size fractions. The correction equation was determined by regressing accepted values of SRMs versus their mean pXRF concentrations(see Knight et al., 2013). Note the regression line for the corrected data is improved.

6.0 Application of pXRF analysis of surficial samples to field studies

Our comparison of the pXRF data with laboratory data (fusion or 4-acid methods), demonstrates that pXRF analyses can provide highly valuable and cost effective information. While the pXRF data does not exactly replicate the laboratory data (in terms of precision and accuracy), the relationship between pXRF data and fusion or 4-acid data is in general highly systematic, and thus can be post-analysis corrected if warranted (Knight et al., 2013). However, for simplicity, we have chosen to display the raw pXRF data as interpolated single element plots using. In this format the elemental anomalies are still observed, as till samples with high pXRF concentration levels are synonymous with high laboratory based analytical concentration levels, and till samples with low pXRF concentration levels are synonymous with low laboratory based analytical concentration levels.

Five representative single element interpolated maps are presented here for Rb, Ba, Cr, Zn and Zr (Figs. 17 to 21), with all maps presented in Appendix D. Note that these maps are based on a relative scale, i.e., the range of concentration level differs for each map, depending on the analytical method and detection limit. The maps were produced using the Natural Neighbor Interpolator of Vertical Mapper operating within MapInfo™. The interpolated grid was created using a 100 m cell size, an aggregation distance of 500 m, and a fixed color profile for the 0, 50^{th} 95^{th}, 98^{th} and 100^{th} percentiles; these parameters are as previously used in Kjarsgaard et al. (2013a, e).

For Rb the pXRF map closely replicates maps generated by fusion or 4-acid methods for both the < 2 mm and < 0.063 mm size fractions (Fig. 17). The aqua regia Rb map differs, with two anomalies adjacent to Ptarmigan Lake and another in the northeast corner of the study area that are not observed in the other Rb maps (Fig. 17). In addition, absolute Rb concentrations determined by aqua regia are significantly lower (< 65%) than by any other method.

The Ba pXRF map also closely replicates maps generated by fusion or 4-acid methods for both < 2 mm and < 0.063 mm size fractions (Fig. 18). The aqua regia Ba map has an

anomaly southwest of Reliance that is not observed on the other Ba maps, and the anomaly in the northeast corner of the study area is not as aerially extensive (Fig. 18). Absolute Ba concentrations determined by aqua regia are significantly lower (< 73%) than by any other method.

For Zr it is problematic to compare the pXRF map to those generated by laboratory methods, since absolute concentration levels of the till samples vary considerably as a function of grain size and analytical method. Importantly, however, the pXRF map has similarities with the maps generated from the 2 mm size fraction fusion data (Fig. 19), whereas the < 0.063 mm size fraction exhibits a number of additional anomalies at the eastern edge of the study area. The 2 mm and < 0.063 mm 4-acid maps mimic the fusion maps, however the anomalies are significantly weaker, as expected due to incomplete zircon dissolution. The aqua regia map does not display the majority of the anomalies evident on the pXRF, fusion and 4-acid maps. This is interpreted as a result of incomplete or no zircon digestion by aqua regia. Absolute Zr concentrations determined by aqua regia are significantly lower (< 90%) than by any other method.

The Cr pXRF map, with a range of 5 – 104 ppm Cr is difficult to compare to maps generated by laboratory methods, in which maximum concentration levels vary considerably, as a function of grain size and analytical method (86 – 239 ppm Cr). Furthermore, the pXRF map was interpolated using only 62 data points (~25% of the sample set), as the majority of data are below the pXRF detection limit. Despite this, the pXRF map and the fusion map for the < 0.063 mm size fraction are similar, but the anomalies on the fusion map are more subtle (Fig. 20). This is consistent with Cr residing mainly in chromite grains, which tends to smaller grain sizes (< 0.20 mm).

The pXRF map for Zn closely replicates maps generated by fusion or 4-acid methods for the < 2 mm size fraction, and is similar to the < 0.063 mm size fraction for fusion, 4-acid and aqua regia. However, the Zn anomaly south of Walmsley Lake, and adjacent to the Hoarfrost River, as exhibited on the fusion and 4-acid Zn maps, is not displayed on the aqua regia or pXRF map (Fig. 21).

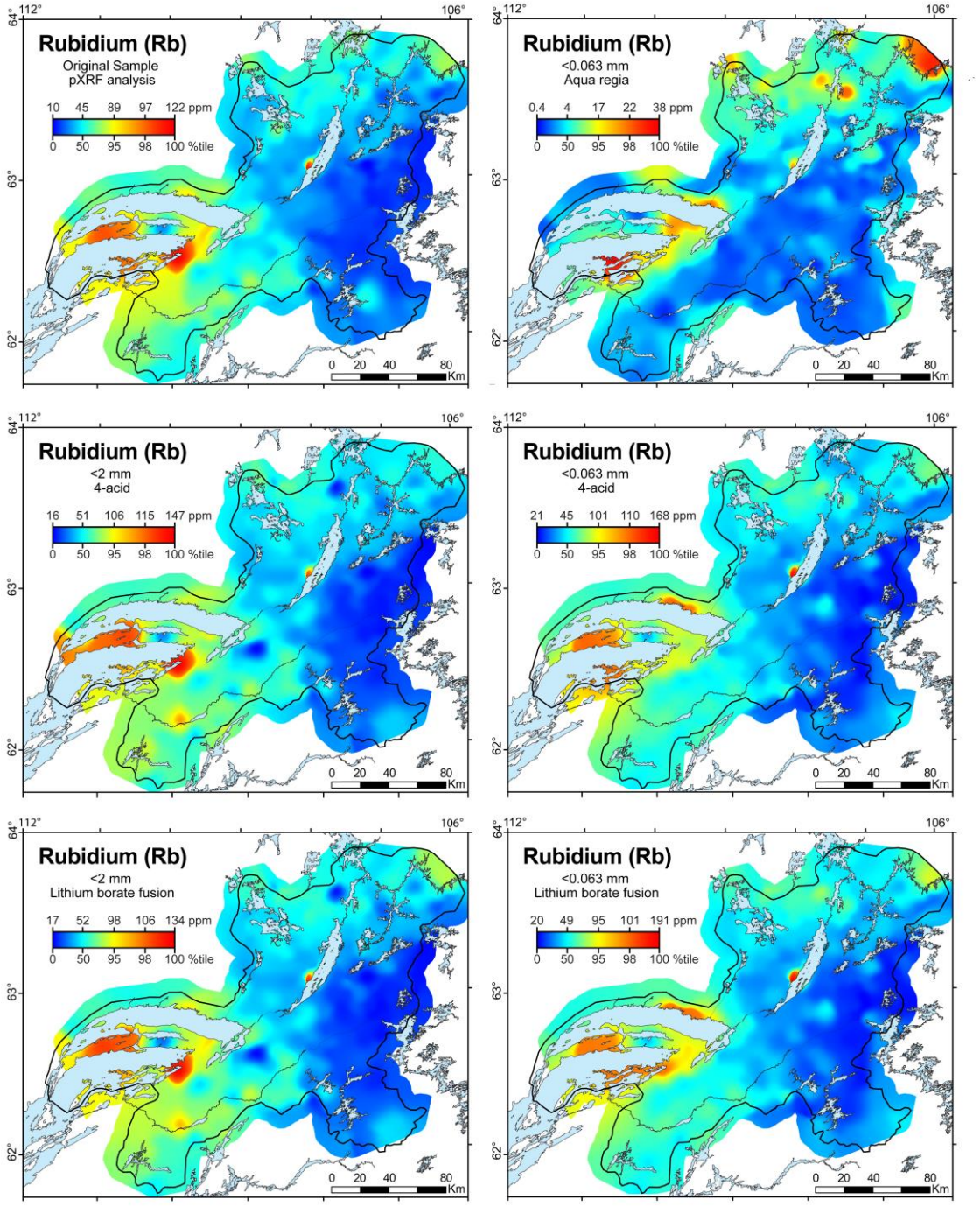

Figure 17. Interpolated single element map for Rb, comparing data from pXRF, with < 0.063 mm data from aqua regia, 4-acid and fusion methods, and < 2 mm data from 4-acid and fusion methods.

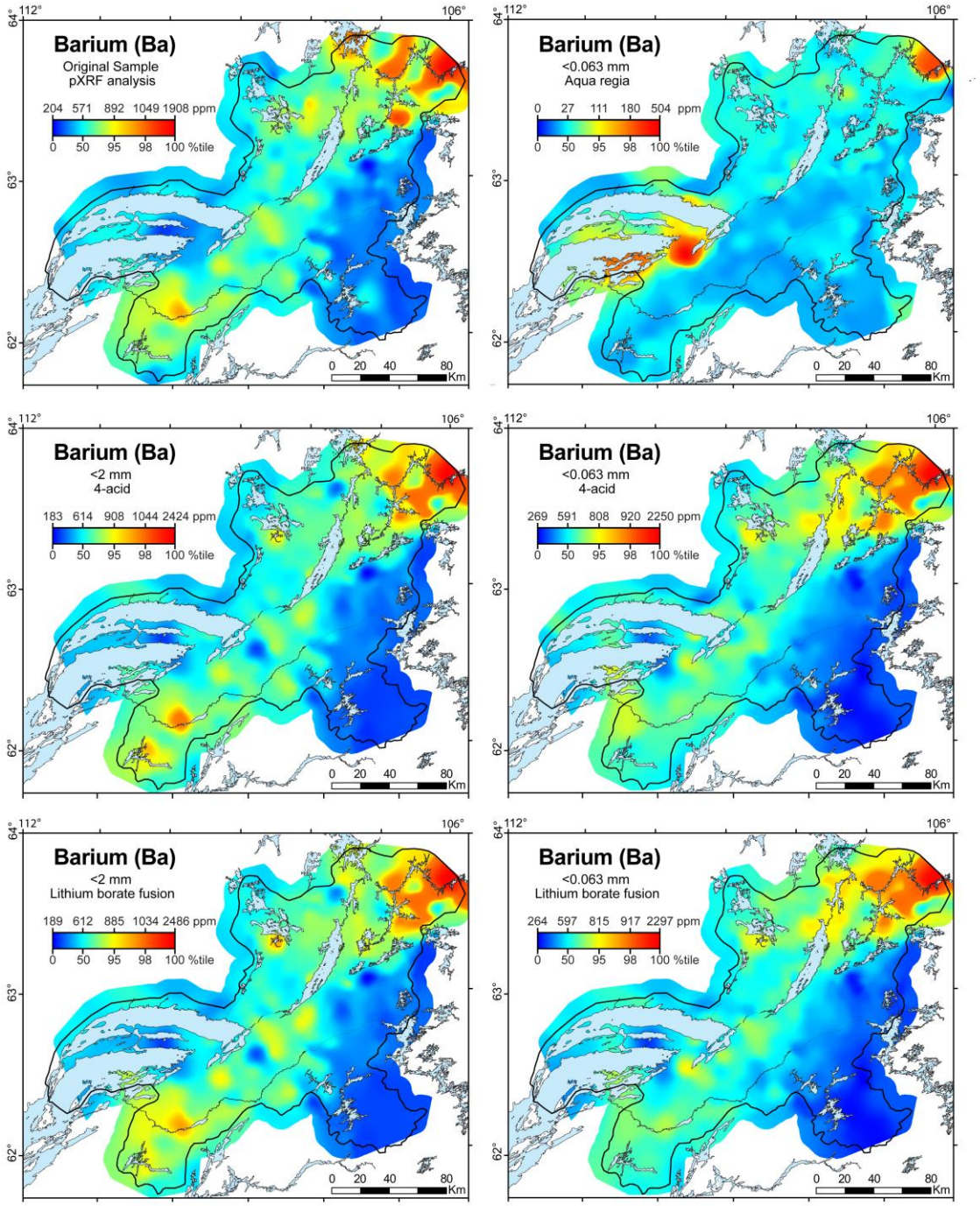

Figure 18. Interpolated map for Ba, comparing data from pXRF, with < 0.063 mm data from aqua regia, 4-acid and fusion methods, and < 2 mm data from 4-acid and fusion methods.

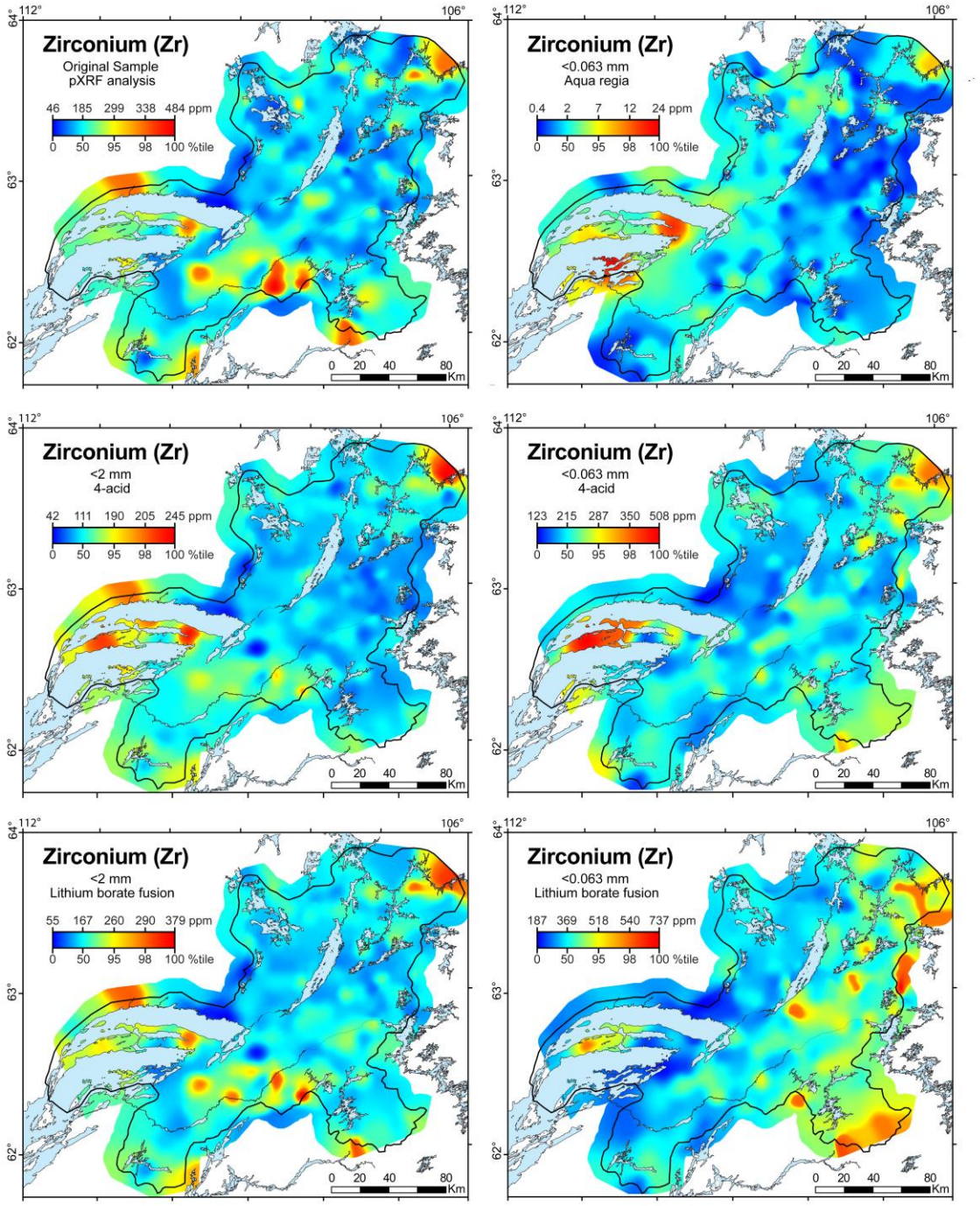

Figure 19. Interpolated map for Zr, comparing data from pXRF, with < 0.063 mm data from aqua regia, 4-acid and fusion methods, and < 2 mm data from 4-acid and fusion methods.

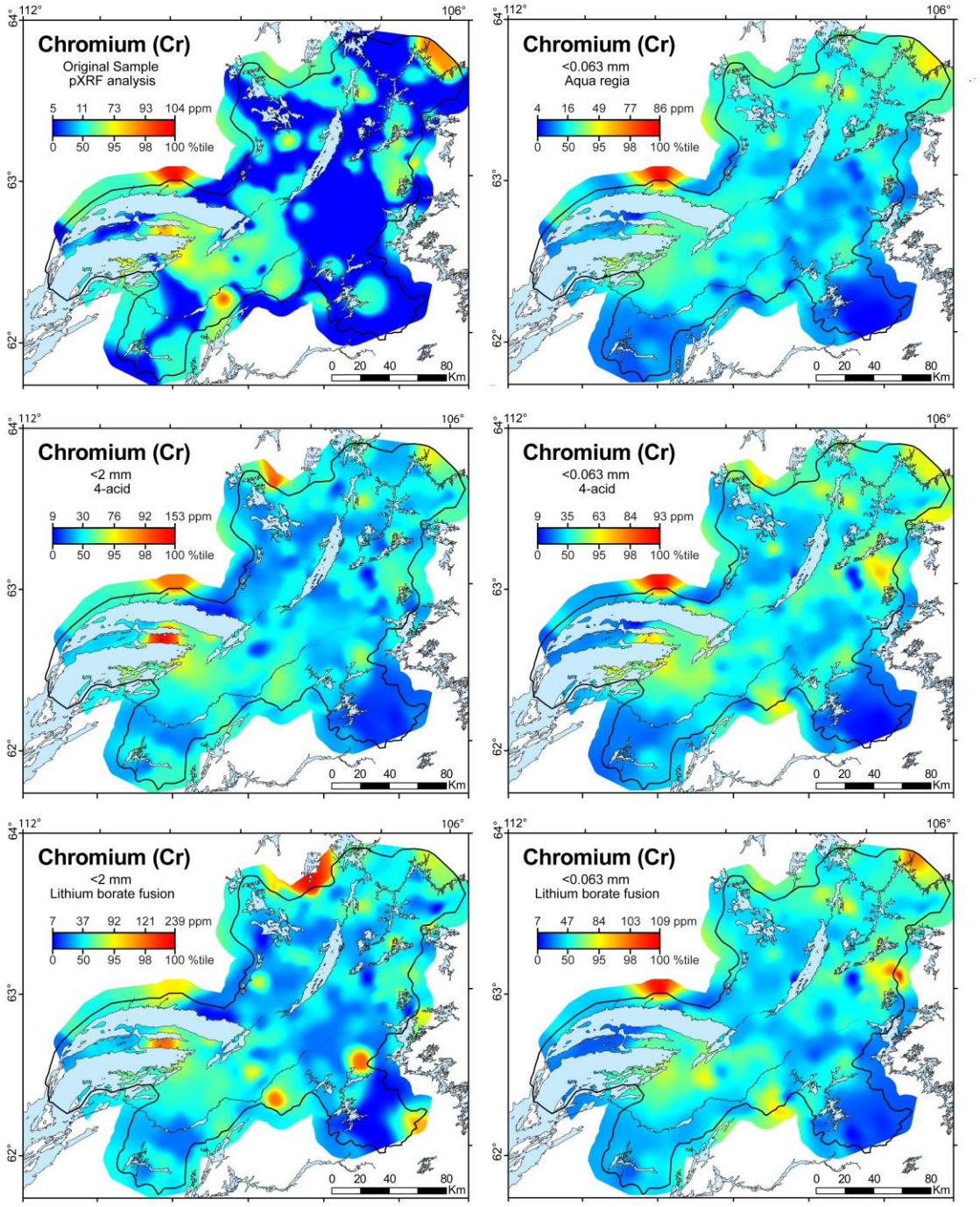

Figure 20. Interpolated map for Cr, comparing data from pXRF, with < 0.063 mm data from aqua regia, 4-acid and fusion methods, and < 2 mm data from 4-acid and fusion methods.

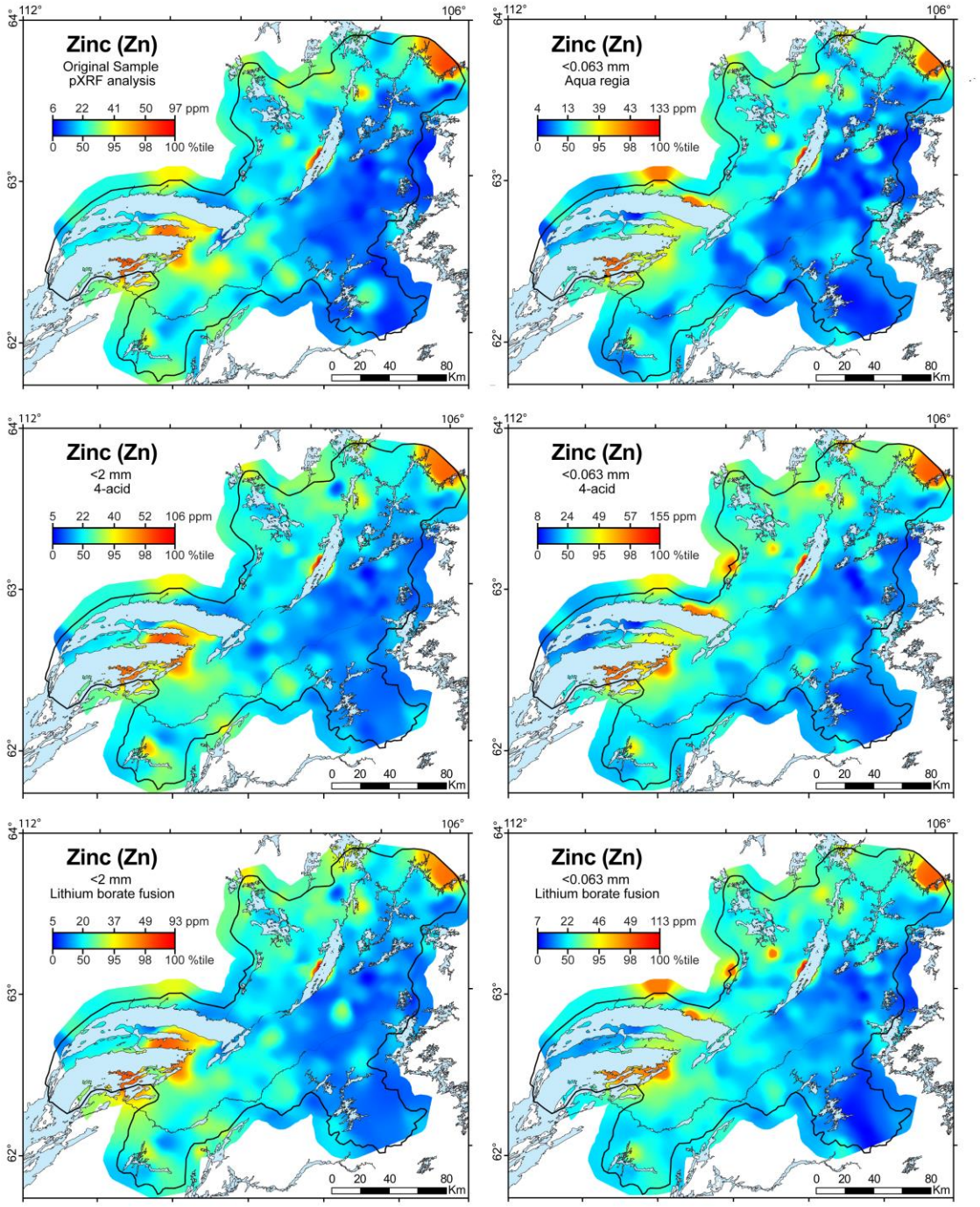

Figure 21. Interpolated map for Zn, comparing data from pXRF, with < 0.063 mm data from aqua regia, 4-acid and fusion methods, and < 2 mm data from 4-acid and fusion methods.

7.0 Sample preparation and analytical protocols for pXRF field studies

The pXRF analyses of this study were performed 'in-house' in Ottawa. A variation of this methodology (drying, sieving to < 2 mm, no shaking) was successfully field tested (Plourde et al., 2013), and it documented the location of several geochemical anomalies for e.g., Ni, Cr, Cu, Pb, Zn, Sr, Ti that were subsequently verified by conventional laboratory analyses (Kjarsgaard et al., 2013a).

Given the results presented in this study, and by Plourde et al. (2013), we suggest the following field protocols for pXRF analysis of surficial sediments:

(1) field collection of a 1 kg till sample, from which a sub-sample for pXRF is taken, using a 100 ml vial,
(2) drying of pXRF sample at 60 ˚C for approximately 1 hour, (clay-rich sediment may require disaggregating),
(3) sieving of pXRF sample to < 2 mm (or 1 mm, depending on diamicton grain size and amount of time available for sieving and cleaning sieves),
(4) returning the dried and sieved sample to a 30 ml vial, attaching lid, inverting of vial and subsequent shaking e.g., with a commercial shaker. In our experience, shaking can be accomplished by placing a box or tray of samples in the storage compartment of a running helicopter for ~30 minutes, or strapped to the back of an ATV and driven for ~30 minutes, or any other device that shakes the sample and enables granular convection to further separate the sample into a clay- and silt-rich fraction,
(5) inverting vials to top up and replacing lid with 4 μm thick Mylar® polyester film,
(6) analysis by pXRF in a test stand, in an environment with minimal temperature and humidity fluctuation (if possible), done in conjunction with a set of suitable SRM's that cover the complete range of expected elements and element concentrations, including a Si blank to check for cleanliness of the test stand environment.

8.0 Discussion/Conclusions

Based on the data presented on the bivariate plots and interpolated single element maps, we suggest that pXRF analyses of dried, non-sieved, shaken (with removal of the coarser sand and pebble fraction) surficial till samples provide valuable information that can be utilized in regional surveys to outline areas with anomalous surficial geochemical signatures. The revised field protocols for sample preparation and analysis, as listed in section 7.0 (that include a preliminary sieving), should further facilitate the detection of anomalous sample sites and geographic localities that can be re-sampled in greater detail during the same field season. These tactics should increase the success of a mineral exploration and/or environmental sampling program.

9.0 Acknowledgements

Eric Grunsky is thanked for his careful and insightful review comments, that proved exceptionally useful, as well as his informal discussions on pXRF and surficial geochemistry. TGI-4 is thanked for funding.

10.0 References

Girard, I., Klassen, R.A., and Laframboise, R.R., 2004. Sedimentology laboratory manual, Terrain Sciences Division. Geological Survey of Canada, Open File 4823, 134 p.

Hall, G.E.M. and McClenaghan, M.B., 2013. Field portable XRF in exploration and mining. Geological Survey of Canada, Open File 7374, p. 75-81.

Kenna, T.C., Nitsche, F.O., Herron, M.M., Mailloux, B.J., Peteet, D., Sritrairat, S., Sands, E., and Baumgarten, J., 2011. Evaluation and calibration of a Field Portable X-Ray Fluorescence spectrometer for quantitative analysis of siliciclastic soils and sediments. Journal of Analytical Atomic Spectrometry, v. 26, p. 395-405.

Kerr, D.E., Knight, R.D., Sharpe, D.R., Cummings, D.I., Russell, H.A.J. and Kjarsgaard, B.A., 2013a. Surficial geology of the proposed National Park Reserve on te East Arm of Great Slave Lake. Chapter 5, *in* Mineral and Energy Resource Assessment for the Proposed Thaidene Nene National Park Reserve in the area of the East Arm of Great Slave Lake, Northwest Territories, (eds.) D.F. Wright, E.J. Ambrose, D. Lemkow and G.F. Bonham-Carter; Geological Survey of Canada, Open File 7196.

Kerr, D.E., Knight, R.D., Sharpe, D.R., Cummings, D.I. and Kjarsgaard, B.A., 2013b. Surficial geology map, East Arm MERA study area. Scale 1:250,000. Digital Supplement 2, *in* Mineral and Energy Resource Assessment for the Proposed Thaidene Nene National Park Reserve in the area of the East Arm of Great Slave Lake, Northwest Territories, (eds.) D.F. Wright, E.J. Ambrose, D. Lemkow and G.F. Bonham-Carter; Geological Survey of Canada, Open File 7196.

Kjarsgaard, B.A., Knight, R.D., Grunsky, E.C., Kerr, D.E., Sharpe, D.R., Cummings, D.I., Russell, H.A.J., Kerswill, J.A., and Wright, D.F., 2013a. Till geochemistry studies of the Thaidene Nene MERA study area, Chapter 10 *in* Mineral and Energy Resource Assessment for the Proposed Thaidene Nene National Park Reserve in the area of the East Arm of Great Slave Lake, Northwest Territories, (eds.) D.F. Wright, E.J. Ambrose, D. Lemkow and G.F. Bonham-Carter; Geological Survey of Canada, Open File 7196.

Kjarsgaard, B.A., Marshall, J., Pearson D.G. Lemkow, D., van Breemen, O., DuFrane, A. and Heaman, L.M., 2013b. Slave Craton Bedrock Geology, Thaidene Nene MERA Study Area. Chapter 2, *in* Mineral and Energy Resource Assessment for the Proposed Thaidene Nene National Park Reserve in the area of the East Arm of Great Slave Lake, Northwest Territories, (eds.) D.F. Wright, E.J. Ambrose, D. Lemkow and G.F. Bonham-Carter; Geological Survey of Canada, Open File 7196.

Kjarsgaard, B.A., Pearson D.G., DuFrane, A., and Heaman, L.M., 2013c. Proterozoic Geology of the East Arm Basin with emphasis on Paleoproterozoic magmatic rocks, Thaidene Nene Mera Study Area. Chapter 3, *in* Mineral and Energy Resource Assessment for the Proposed Thaidene Nene National Park Reserve in the area of the East Arm of Great Slave Lake, Northwest Territories, (eds.) D.F. Wright, E.J. Ambrose, D. Lemkow and G.F. Bonham-Carter; Geological Survey of Canada, Open File 7196.

Kjarsgaard, B.A., Lemkow, D. and Tella, S., 2013d. Bedrock geology map, East Arm MERA study area. Scale 1:250,000. Digital supplement 1, *in* Mineral and Energy Resource Assessment for the Proposed Thaidene Nene National Park Reserve in the area of the East Arm of Great Slave Lake, Northwest Territories, (eds.) D.F. Wright, E.J. Ambrose, D. Lemkow and G.F. Bonham-Carter; Geological Survey of Canada, Open File 7196.

Kjarsgaard et al., Knight, R.D., Plourde, A.P., Sharpe, D.R. and J-E. Lesemann, 2013e. Geochemistry of till samples, NTS 75-I, 75-J, 75-O, 75-P (Mary Frances Lake - Whitefish Lake - Thelon River area), Northwest Territories. Geological Survey of Canada, Open File 7351, 27 p.

Knight, R.D., Kjarsgaard, B.A., Plourde, A.P. and Moroz, M., 2013. Portable XRF spectrometry of standard reference materials with respect to precision, accuracy, instrument drift, dwell time optimization, and calibration. Geological Survey of Canada, Open File 7358, 45 p.

Kudrolli, A., 2004. Size separation in vibrated granular matter. Reports on Progress in Physics, v.67, n.3, p. 209-247.

LeMaitre, R.W., 1982. Numerical petrology. Elsevier, New York, 281 p.

Lynch, J., 1996. Provisional elemental values for four new geochemical soil and till reference materials, TILL-1, TILL-2, TILL-3 and TILL-4. Geostandards Newsletter, v. 20, n. 2, p. 277-287.

McLaren, T.E., Guppy, C.N., Forster, N., Grave, P., Lisle, L.M., and Bennett, J.W., 2011. Rapid, non-destructive total elemental analysis of Vertisol soils using portable X-ray fluorescence. Soil Society of America Journal, v. 76, p. 1436-1445.

Morris, P.A., 2009. Field-portable X-ray fluorescence analysis and its application in GSWA. Geological Survey of Western Australia, Record 2009/7, 23p.

Plourde, A.P., Knight, R.D., Kjarsgaard, B.A., Sharpe, D.R., and Lesemann, J-E., 2013. Portable XRF spectrometry of surficial sediments, NTS 75-I, 75-J, 75-O, 75-P (Mary Frances Lake - Whitefish Lake - Thelon River area), Northwest Territories. Geological Survey of Canada, Open File 7408, 25 p.

Sharpe, D.R., Russell, H.A.J. and Knight, R.D., 2013. Glaciofluvial features and their significance in the proposed national Park Reserve, East Arm of Great Slave Lake. Chapter 6, *in* Mineral and Energy Resource Assessment for the Proposed Thaidene Nene National Park Reserve in the area of the East Arm of Great Slave Lake, Northwest Territories, (eds.) D.F. Wright, E.J. Ambrose, D. Lemkow and G.F. Bonham-Carter; Geological Survey of Canada, Open File 7196.

Tella, S., Kjarsgaard, B.A. and Lemkow, D., 2013. Bedrock geology of the western Churchill Province and Taltson and Thelon magmatic-tectonic zones, Thaidene Nene NERA Study Area. Chapter 1, *in* Mineral and Energy Resource Assessment for the Proposed Thaidene Nene National Park Reserve in the area of the East Arm of Great Slave Lake, Northwest Territories, (eds.) D.F. Wright, E.J. Ambrose, D. Lemkow and G.F. Bonham-Carter; Geological Survey of Canada, Open File 7196.

Weindorf, D.C., Zhu, Y., Chakraborty, Somsubhra, Bakr, N. and Huang, B., 2012. Use of portable X-ray fluorescence spectrometry for environmental quality assessment of peri-urban agriculture. Environmental Monitoring and Assessment, v.184, p. 217-227.

Weltje, G.J. and Tjallingii, R., 2008. Calibration of XRF core scanners for quantitative geochemical logging of sediment cores: theory and application. Earth and Planetary Science Letters, v. 274, p. 423-428.

Wills, B.A., 1979. Mineral processing technology: An Introduction to the practical aspects of ore treatment and mineral recovery. Pergamon Press, New York, 418 p.

Wilson, S.A., Briggs, P.H., Brown, Z.A., Taggart, J.E. and Knight, R., 1999. Collection, preparation and testing of NIST hard rock mine waste reference material SRM 2780. USGS Open File Report 99-370, 15 p.

York, D., 1966. Least squares fitting of a straight line with correlated errors. Earth and Planet6ary Science Letters, v. 5, 320-324.